# Numerical investigation of a first-stage stator turbine blade subjected to $NH_3$-$H_2$/air combustion flue gases

Odi Fawwaz Alrebei[1,*], Laurent M. Le Page[2], Sally Hewlett[3], Yusuf Bice[4], Abdulkarem Amahmed[1]
[1]Hamad Bin Khalifa University, Qatar Environment and Energy Research Institute (QEERI), Doha, 34110, Qatar
[2]Oxford Thermofluids Institute, Oxford University, Oxford, OX2 OES, UK
[3]Cardiff University, School of Engineering, Queen's Buildings, 14-17 The Parade, Cardiff CF24 3AA, UK
[4]Division of Sustainable Development, College of Science and Engineering, Hamad Bin Khalifa University, Qatar Foundation, Doha, Qatar
[*]Correspondence: Telephone: 0097470016088, Email: oalrebei@hbku.edu.qa

## ABSTRACT

Blending ammonia with hydrogen has the potential to replace conventional hydrocarbon fuels of jet engines and gas turbines to reduce carbon emissions. Previous research on the 70%$NH_3$-30%$H_2$ (vol%) fuel blend characterized its cycle efficiency and emissions, however, the thermal and aerodynamic effects of the $NH_3$-$H_2$/air combustion flue gases on the turbine blades were not identified. Therefore, the novelty of the analysis presented herein appears in characterizing such effects of the $NH_3$-$H_2$/air combustion flue gases on a generic turbine blade model using CFD simulation for lean ($\Phi$ = 0.75), stoichiometric ($\Phi$ = 1.00), and rich ($\Phi$ = 1.25) equivalence ratios, which are compared to a $CH_4$/air combustion flue at $\Phi$ = 0.75, 1.00 and 1.25, respectively. Based on the obtained results, a cooling channel's ability to reduce the blade's temperature was negligible based on the temperature difference between the leading edge of the turbine blade and the temperature of the combustion flue gas at the inlet. As the combustion equivalence ratio was increased from 0.75 to 1.25, a second shockwave forms at the leading-edge surface, projecting across the blade's lower edge. The formation of the second shockwave was found to be increasingly significant for the $NH_3$-$H_2$/air mixture on the downstream flow when compared to a $CH_4$/air flue gas. Furthermore, increasing the $NH_3$-$H_2$/air equivalence ratio improved the blade's ability to increase the average overall outlet Mach number compared to the inlet flow. Flow separation near the trailing edge remained relatively unaffected with increasing equivalence ratio. However, separation near the leading edge at the blade's lower edge becomes more significant for the $NH_3$-$H_2$/air combustion flue gases compared to $CH_4$/air combustion, causing a large circulation zone under the blade's lower surface due to the higher kinematic viscosity for the $NH_3$-$H_2$ fuel to the $CH_4$ fuel (i.e., $2.06 \times 10^{-5}$ $m^2/s$ and $1.75 \times 10^{-5}$ $m^2/s$, respectively). The circulation induces a higher viscous force and fluid inertia in the boundary layer, causing higher levels of separation. Turbulence intensity was also found to be significantly increased for the $NH_3$-$H_2$/air flow to that of the $CH_4$/air combustion flue gases with increasing equivalence ratio.

**KEYWORDS:** $NH_3$-$H_2$/air combustion, turbine blade cooling, aerodynamic analysis, thermal analysis, Computational Fluid Dynamics

## 1. INTRODUCTION

While hydrogen is predicted to play a significant role in future power generation, it still faces significant challenges in terms of distribution and storage [1]. Despite the global effort to promote hydrogen as an alternative fuel in the power generation industry, large expenditures are still required to make it more widely available as a liquefied fuel [2]. Hydrogen liquefaction is not yet economically viable for power generation purposes using current technologies as the price of required equipment for hydrogen liquefaction remains prohibitively expensive for mass production. In addition, storage of

hydrogen presents a high risk of explosion if inadvertently oxidized [3]. As a result, ammonia has been proposed as a hydrogen storage vector in the literature as converting hydrogen to ammonia allows for liquefaction under mild pressure and temperature conditions (similar to propane storage) and considerably reduces flammability risk [3-4]. Japanese experts declared in 2021 that a 40-MW gas turbine running entirely by ammonia is nearing completion [5]. A gas turbine of this kind will make it easier to decarbonize small-sized power plants for industrial uses. A number of papers have also been made about using $NH_3$ to run small power plants [6,7]. The principle of an $NH_3$-fired chemically recuperated gas turbine (CRGT) was thermodynamically studied using Aspen-HYSYS in a previous paper by Pashchenko et al. [8], and it was discovered that 43% of the waste heat can be recovered. Additionally, Verkhivker and Kravchenko performed a thermodynamic analysis of a cogeneration plant using steam methane reforming-based thermo- chemical recuperation [9]. The authors suggested that steam from a steam turbine's high-pressure cylinder be used for reforming. According to calculations by Verkhivker and Kravchenko, a cogeneration plant with thermo-chemical recuperation can achieve an energy efficiency of up to 90%. The technoeconomic comparison and multi-objective optimization findings of the combined gas turbine and organic Rankine cycle power production system with thermochemical recuperation based on steam methane reforming and thermophysical recuperation were also presented by Sadeghi et al. [10].

Pure ammonia-air combustion does not meet industrial power needs within acceptable $NO_x$ emission margins. While industrial standards for $NO_x$ emissions can be as low as 10 ppm, ammonia-air combustion without significant post-combustion $NO_x$ reduction (e.g. via the use of thermal de-$NO_x$ treatments) produces $NO_x$ concentrations in the hundreds or even thousands of ppm [10-12]. The US National Ambient Air Quality Standard (NAAQS) for nitrogen oxides is an annual standard at a level of 53 ppb [10-12]. When internal combustion engines are fueled with pure ammonia, the chemical reaction rate is slower than traditional fuels due to its high ignition temperature and low flame velocity. For example, for the pure $NH_3$ fuel, the flame speed is decreased by a factor of 2.8 compared to fuel 70 % $NH_3$ - 30 % $H_2$ (vol. %) fuel blend [12]. This slow chemical reaction rate can cause ammonia to be discharged from the exhaust without burning [11-12]. Therefore, mixing ammonia with hydrogen produces a more reactive fuel blend than pure ammonia. As a carrier of hydrogen, a portion of the ammonia fuel can be 'cracked' to produce a hydrogen stream (and a nitrogen stream). However, $NO_x$ emissions are one of the major drawbacks of combining $NH_3$ and $H_2$ for power generation. The 70 % $NH_3$-30 % $H_2$ (vol. %) blend has shown the best emissions performance among several alternatives in the literature [3,12-13] and has been adopted for further examination in this work.

The thermal and aerodynamic impacts of $NH_3$-$H_2$/air combustion flue gases on turbine blades have not been identified in prior research [3,10-13]. To minimise engine failure or abnormal combustion, it is critical to evaluate the effect of combustion flue gases on turbine blades for any proposed alternative fluid or fuel. One of the most prevalent techniques to improve gas turbine efficiency is to raise the turbine inlet turbine temperature (TIT). However, this presents a problem for the turbine airfoils as they need to be able to withstand these higher temperatures. For industrial gas turbines, the TIT is predicted to reach 2000 K by 2030 and considerably higher for aircraft engines [13-14]. Internal and exterior film cooling of gas turbine airfoils are two of the most common approaches for improving their ability to endure such high temperatures [14]. The first stage of the turbine section of high-performance aero-engines or high-pressure ratio industrial gas turbines used as land-based prime movers may have a transonic flow region, where shock waves can form. Wakes and shock waves are produced in the flow by the stator-rotor contact in a transonic turbine [15]. The passing shock wave is the principal cause of flow turbulence in the first stage turbine, according to Doorly and Oldfield [16]. The influence of shock waves and periodic wakes on cooling efficiency on the leading edge of a blunt body has been reported such that cooling efficacy reduces in the region where the periodic wakes and shock waves originate [17]. Ochs et al. [18] investigated the influence of a stator's trailing edge shock wave on the film cooling effectiveness over the suction side of a downstream gas turbine blade. Significant detail on the fluid dynamics was reported that included total

cascade losses produced by developed boundary layers, shocks, trailing edge wakes, and coolant mixing with the mainstream, which have been identified as the most significant contributors to total losses, which has also been noted by Rehder [19].

Several numerical studies have been conducted on this topic due to the difficulty and high cost of conducting experiments to evaluate turbine blades' thermal and aerodynamic impacts. The shock fluctuations induced by shocks at 15% blade height are twice as significant as those caused by shocks at 85% blade height, according to de la Loma et al. [20]. Abhari et al. [21-22] and Schlienger et al. [23] compared experimental data with 2D numerical results on the surfaces of both cooled and uncooled turbine blades using the conventional k-turbulence model. The Shear Stress Transport (SST) model with two modifications, the SST with Curvature Correction (SSTCC) and the SST-($\gamma$ –Re$\theta$ ), were employed by Ragab et al. [24] to forecast the film cooling effectiveness in a transonic turbine vane. The differences between the two models' results were negligible. Xu et al. [25-27] compared the computational results of various turbulence models (k-ε, SST k-ω, and the Reynolds-Stress Models (RSM)) with experimental data transonic conditions and Hunter [28] for supersonic conditions. They reported that the SST k-ω, RSM, and k-ε models agreed better with the experimental data. As a result, they studied transonic and supersonic conditions using the k-model, which is less computationally expensive.

Whereas previous literature provides abundant information about the thermal and aerodynamic behavior over turbine blades for the combustion flue gases of conventional fuels, using alternative fuels such as the 70% $NH_3$-30 % $H_2$ (vol%) blend requires investigating their unique thermal and aerodynamic effects (such as fluid composition, temperature, pressure, and velocity) on the turbine blade. Therefore, novelty of the analysis presented herein appears in characterizing thermal and aerodynamic effects of the $NH_3$-$H_2$/air combustion flue gases of the 70% $NH_3$-30 % $H_2$ (vol%) blend on a generic turbine blade model by combining two simulation stages; 1) CHEMKIN-PRO to set accurate boundary conditions for the 2) CFD analysis in ANSYS CFX, shown in the subsequent section. Table 1 provides a comparison with literature to highlight the outstanding findings of this work.

**Table 1.** The effort in literature to utilize ammonia blends as an alternative fuel.

| Reference | Scope of work | Findings | Limitations |
|---|---|---|---|
| [3] | Experimental and numerical characterization of a $NH_3$-$H_2$ fuel blend in premixed combustion | Acceptable flammability limits (similar to the pure $CH_4$ combustion) were found. | • High $NO_x$<br>• Numerical results were obtained from an equilibrium-based computational tool (Gaseq), ignoring the considerable impact of the swirling flow hydrodynamics and complex heat transfer phenomena. |
| [4] | A chemical-kinetic based study (Chemkin) has been conducted to determine the Quantitative Reaction Path Diagrams (QRDP) of a 70-30 (vol%) $NH_3$-$H_2$ fuel blend. | Differences and similarities in QRDP have been identified for five chemical kinetic models in humidified ammonia combustion | • Results were displayed for a single equivalence ratio (i.e., 1.2).<br>• The overall performance of a gas turbine at the 1.2 equivalence ratio has not been taken into consideration. |
| [12] | Developing a kinetic model to predict the reaction mechanism for oxidation of the $NH_3$-$H_2$ blends | Enriching the oxidizer stream by 30% of pure O2 has the same effect on increasing flame speed by a factor 2.8 as increasing the hydrogen content (i.e., to 30%) in the | • The overall performance of a gas turbine has not been taken into consideration.<br>• The aspect of turbine overheating has not been considered when increasing |

| | | | |
|---|---|---|---|
| | | fuel stream. | the hydrogen content. |
| [29] | Determining the cycle efficiency of a gas turbine that utilizes the 70%$NH_3$-30%$H_2$ (vol%) fuel blend at a variety of equivalence ratios | Comparing efficiency and emission performances between the $CH_4$/air and $NH_3$-$H_2$/air gas turbines, the latter was found to have a higher efficiency performance at Φ=0.75 | • Characterizing the thermal and aerodynamic effects of the $NH_3$-$H_2$/air combustion flue gases on turbine blades was not considered. |
| This paper | Analysis presented herein seeks to characterize these thermal and aerodynamic effects of the $NH_3$-$H_2$/air combustion flue gases on a generic turbine blade model at a variety of equivalence ratios | The recommended and the To-Be-Avoided equivalence ratios have been obtained with respect to the studied parameters o (the maximum temperature of the turbine blade, the pressure losses, the blade's capability of increasing $M_{out}$ and turbulent kinetic energy). More details are found in the results and discussion sections. | • Discussed in the conclusion section |

## 2. SETUP

A previous paper by Alrebei et al. [29] presented a standard gas turbine cycle analysis code that has been utilized to perform a comparative analysis of gas turbines fueled with both $NH_3$-$H_2$/air and $CH_4$/air, thus highlighting the operating conditions under which $NH_3$-$H_2$/air gas turbines show higher performance when compared to $CH_4$/air gas turbines. Comparing efficiency and emission performances between the $CH_4$/air and $NH_3$-$H_2$/air gas turbines, the latter was found to have a higher efficiency performance at Φ< 0.75. The authors also identified an equivalence ratio (Φ) of 1.25 for minimized emissions. The efficiency and emission performance of the 70%$NH_3$-30%$H_2$ (vol%) blend dictated the equivalence ratio range investigated here (i.e. 0.75 to 1.25). Although in previous research [3, 8, 12-13, 29] of the 70% $NH_3$ - 30% $H_2$ (vol%) blend the cycle efficiency and the emissions have been characterized, thermal and aerodynamic effects of the $NH_3$-$H_2$/air combustion flue gases on the turbine blades were not identified. Analysis presented herein seeks to characterize these thermal and aerodynamic effects of the $NH_3$-$H_2$/air combustion flue gases on a generic turbine blade model. The selected case of study to test the thermal and aerodynamic effects of the combustion flue gases is illustrated in Figure 1, and the blade dimensions are specified in Table 2.

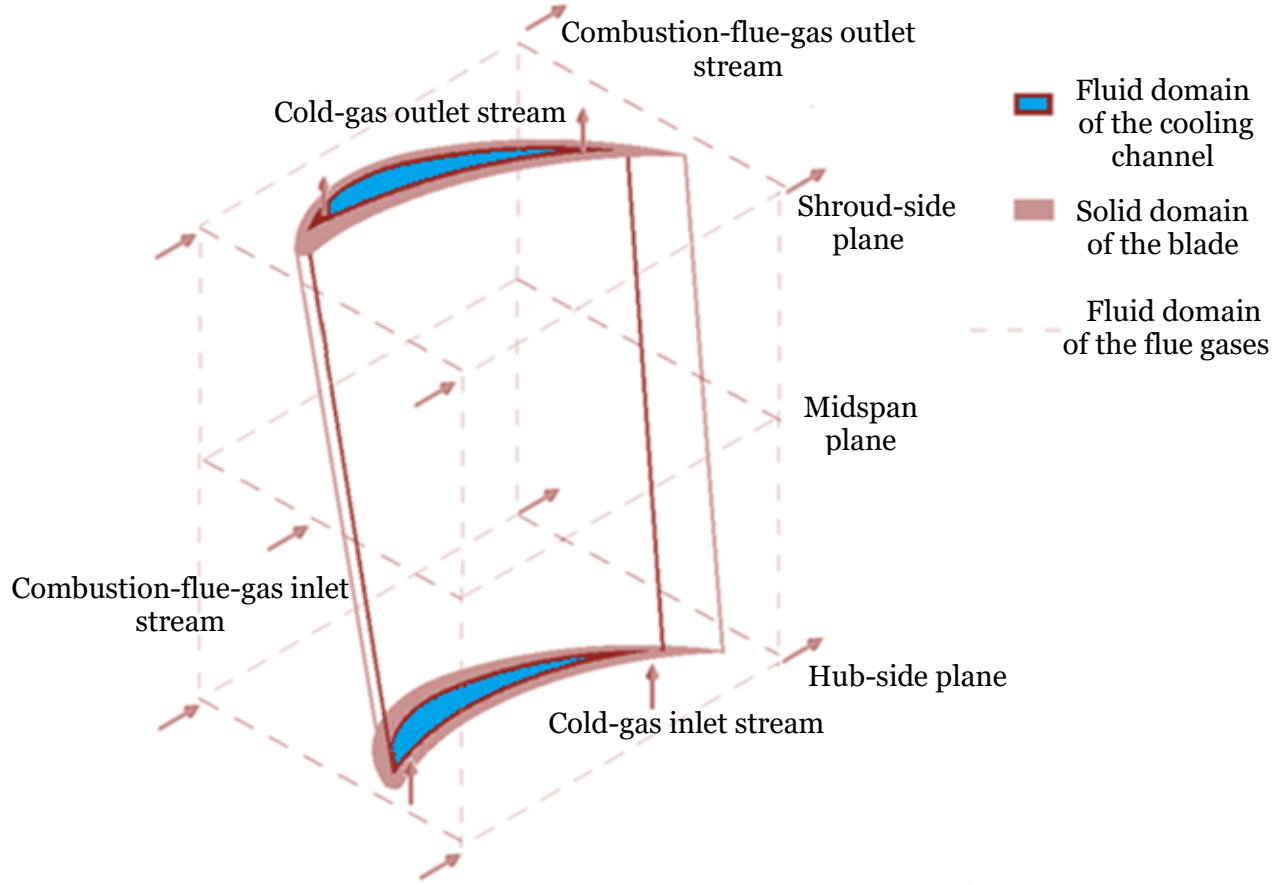


**Figure 1.** Schematic of the turbine blade.

The blade model is exposed to the combustion flue gases and cooled internally through a cooling channel. Inlet conditions and the combustion conditions for general regions about the blade are summarised in Table 3. The flue gas conditions and compositions are specified in Table 3 and Table 4, respectively. The post-combustion flue gas conditions (i.e. temperature, pressure, velocity and composition) entering the blade model, were obtained by utilizing CHEMKIN-PRO, a chemical kinetics simulator that models idealized reacting flows. The chemical reaction mechanism used in the simulator was developed by Okafor et al. [30]. This mechanism provides the necessary ammonia and methane reaction chemistry and has been verified for modeling ammonia combustion [29, 30].

**Table 2.** The geometry of the generic turbine blade.

| Shroud-side | | |
|---|---|---|
| Edge | X location Interval [mm] | Y (X) location [mm] |
| Blade-upper edge | [3.78-48] | $(-4\times10^{-08})x^6 + (6\times10^{-06})x^5 + (0.010)x^3 - (0.193)x^2 + (2.306)x + (22.41)$ |
| Blade-lower edge | [3.78-48] | $(3\times10^{-08})x^6 - (4\times10^{-06})x^5 - (0.005)x^3 + (0.070)x^2 - (0.276)x + (28.26)$ |
| Cooling-channel upper edge | [7.5-43.76] | $(4\times10^{-10})x^6 - (7\times10^{-07})x^5 + (8\times10^{-05})x^4 - (0.003)x^3 + (0.026)x^2 + (0.642)x + (25.85)$ |
| Cooling-channel lower edge | [7.5-43.76] | $(3\times10^{-08})x^6 - (5\times10^{-06})x^5 - (0.010)x^3 + (0.168)x^2 - (1.416)x + (35.69)$ |
| Hub-Side | | |
| Blade-upper edge | [2.32-47.275] | $(-4\times10^{-08})x^6 + (6\times10^{-06})x^5 + (0.009)x^3 - (0.159)x^2 +$ |

| | | | |
|---|---|---|---|
| | | (2.298)x + (1.467) | |
| Blade-lower edge | [2.32-47.275] | $(4\times10^{-08})x^6$–$(5\times10^{-06})x^5$ - $(0.006)x^3$ + $(0.050)x^2$ + (0.569)x + (4.511) | |
| Cooling-channel upper edge | [7-45] | $(-2\times10^{-08})x^6$ + $(3\times10^{-06})x^5$ + $(0.0050x^3$–$(0.111)x^2$ + (2.075)x + (0.754) | |
| Cooling-channel lower edge | [7-45] | $(-1\times10^{-08})x^6$ + $(2\times10^{-06})x^5$ + $(0.004)x^3$–$(0.080)x^2$ + (1.319)x + (4.618) | |
| Blade height (Hub to shroud) [mm] | | | |
| 65 | | | |
| Hot Fluid Domain | X [mm] | Y [mm] | Z[mm] |
| | 50 | 40 | 65 |
| The corresponding coordinate system and dimensions of the blade | | | |

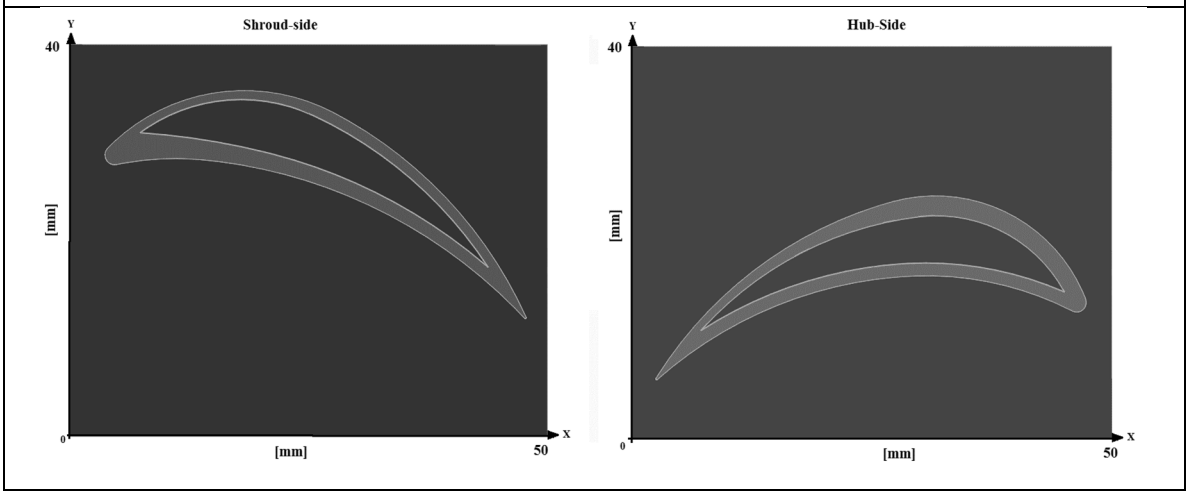


**Table 3.** CHEMKIN-PRO model setup.

| Parameter | Condition |
|---|---|
| Compressor inlet temperature ($T_{01}$) [K] | 300 |
| Combustion chamber premixed inlet temperature ($T_{02}$) [K] | 485 |
| Compressor pressure ratio ($\frac{P_{02}}{P_{01}}$) | 4 |
| Compressor inlet pressure ($P_{01}$)[atm] | 1 |
| Compressor isentropic efficiency ($\varepsilon_c$) | 0.85 |
| Equivalence Ratio (Φ) | 0.75, 1.00, 1.25 |
| Corresponding $CH_4$ flow rate $\dot{m}_f$ to Φ [kg/s] | 0.11676 |
| Corresponding $NH_3$-H2 flow rate $\dot{m}_f$ to Φ [kg/s] | 0.2685 |
| Primary airflow rate ($\dot{m}_{a,p}$) [kg/s] | 2 |

The CHEMKIN-PRO model used for the gas turbine modeling was a gas turbine reactor network available in the program's sample library. This template has been modified for a single premixed inlet stream, as shown in Figure 2. The model consists of three adiabatic Perfectly Stirred Reactors (PSRs) to simulate the mixing, flame, and recirculation zones with 20% recirculation, as recommended by [3, 8, 12-13, 29]). Following the assumptions adopted by Aalrebei et al. [29], the residence times of the gas turbine template used are 0.0005 s, 0.0015 s, and 0.0015 s for the mixing, flame, and recirculation zones, respectively. In addition, as shown in Figure 2, data has been plotted from an adiabatic Plug Flow Reactor (PFR) using the default dimensions of the gas turbine template (with a diameter of 10 cm and a length of 5 cm). The outlet conditions of the combustion chamber generated by the CHEMKIN-PRO model generate the necessary inlet boundary conditions and flue gas compositions (Table 4 and 5) to perform the CFD modeling of the turbine blades. The CFD simulation was performed with the ANSYS 2020

CFX package [31] using a virtual desktop machine with an Intel® Core™ i7-7700 CPU.

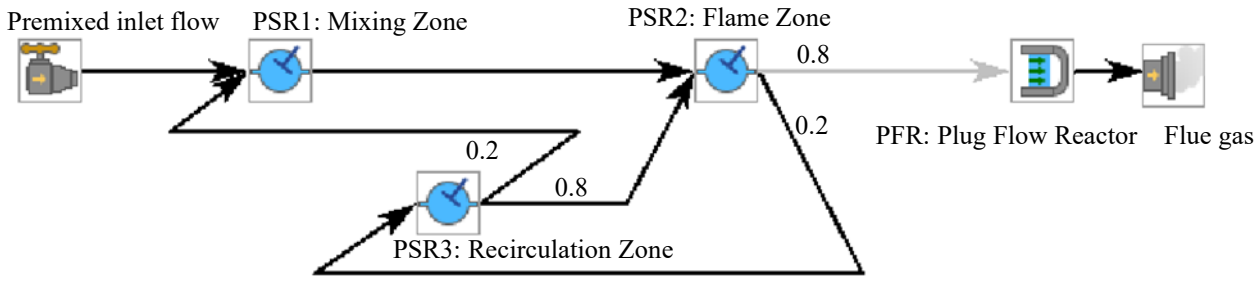


**Figure 2.** CHEMKIN-PRO model (Perfectly Stirred Reactor (PSR), Plug Flow Reactor (PFR)).

**Table 4.** The boundary conditions of the CFD model obtained from the CHEMKIN-PRO model.

| Hot-flue gas | | | | | | |
|---|---|---|---|---|---|---|
| Equivalence ratio | Temperature [K] | | Pressure [atm] | | Velocity [m/s] | |
| | NH3-H2/air | CH4/air | NH3-H2/air | CH4/air | NH3-H2/air | CH4/air |
| 1.25 | 2138.7 | 2216.3 | 3.93 | 3.94 | 569.7 | 481.5 |
| 1 | 2238.1 | 2329.4 | 3.93 | 3.93 | 545.2 | 477.7 |
| 0.75 | 1989.1 | 2056.4 | 3.94 | 3.93 | 451.7 | 407.2 |
| Cooling gas | | | | | | |
| -- | 485 | 485 | 3.94 | 3.94 | 50 | 50 |

**Table 5.** The combustion flue gas compositions of the CFD model are obtained from the CHEMKIN-PRO model.

| | | Mass fractions [%] | | | | | |
|---|---|---|---|---|---|---|---|
| $\Phi$ | Combustion type | $H_2$ | $O_2$ | $H_2O$ | $N_2$ | $NH_3$ | OH |
| 1.25 | $NH_3$-$H_2$/air | 0.624 | 0.00118 | 22.49796 | 76.65688 | 0.0805 | 0.0268 |
| | | NO | $N_2O$ | $NO_2$ | CO | $CO_2$ | $CH_4$ |
| | | 0.111 | 0.00168 | 0.0000018 | 0 | 0 | 0 |
| | $CH_4$/air | $H_2$ | $O_2$ | $H_2O$ | $N_2$ | $NH_3$ | OH |
| | | 0.265 | 0.00893 | 12.93707 | 71.27837 | 0.00005 | 0.0762 |
| | | NO | $N_2O$ | $NO_2$ | CO | $CO_2$ | $CH_4$ |
| | | 0.0383 | 0.00001 | 0.0000018 | 5.91503 | 9.48105 | 0.00000002 |
| 1 | $NH_3$-$H_2$/air | $H_2$ | $O_2$ | $H_2O$ | $N_2$ | $NH_3$ | OH |
| | | 0.08258 | 0.20347 | 22.20354 | 75.87277 | 0.54688 | 0.20644 |
| | | NO | $N_2O$ | $NO_2$ | CO | $CO_2$ | $CH_4$ |
| | | 0.68285 | 0.0000006 | 0.20148 | 0 | 0 | 0 |
| | $CH_4$/air | $H_2$ | $O_2$ | $H_2O$ | $N_2$ | $NH_3$ | OH |
| | | 0.00442 | 0.78496 | 12.02134 | 72.30302 | 0 | 0, 0.28298 |
| | | NO | $N_2O$ | $NO_2$ | CO | $CO_2$ | $CH_4$ |
| | | 0.059 | 0.00005 | 0.00003 | 1.20793 | 13.33627 | 0 |
| 0.75 | $NH_3$-$H_2$/air | $H_2$ | $O_2$ | $H_2O$ | $N_2$ | $NH_3$ | OH |
| | | 0.00176 | 4.822 | 17.873 | 76.326 | 0 | 0.123 |
| | | NO | $N_2O$ | $NO_2$ | CO | $CO_2$ | $CH_4$ |
| | | 0.838 | 0.0141 | 0.00214 | 0 | 0 | 0 |
| | $CH_4$/air | $H_2$ | $O_2$ | $H_2O$ | $N_2$ | $NH_3$ | OH |
| | | 0.00173 | 5.59096 | 9.38421 | 73.27299 | 0 | 0.1369 |
| | | NO | $N_2O$ | $NO_2$ | CO | $CO_2$ | $CH_4$ |
| | | 0.0064 | 0.00002 | 0.07205 | 0.07205 | 11.46271 | 0 |
| Note: components with a mass fraction of less than $1 \times 10^{-11}$ have been neglected. | | | | | | | |

To ensure that the simulation results are independent of the mesh size, a sufficient number of elements were tested. The results are presented in Figure 3 for a coarse grid (2,000,000 elements), a standard grid (4,000,000 elements), a fine grid (6,000,000 elements) and a very fine grid (8,000,000 elements). The mesh sensitivity analysis was performed for the mid-span plane (as it corresponds to the spatially averaged solution) for the $NH_3$-$H_2$/air case study. An equivalence ratio of 0.75 was used, as this case was recommended by [29]). At around $6.3 \times 10^6$ elements, the results become relatively insensitive to the mesh size (i.e., the relative errors of the velocity and total temperature at $6.3 \times 10^6$ elements were approximately 1% compared to the selected mesh size of $8.1 \times 10^6$ elements). As there was no significant additional computational cost, the mesh size of $8.1 \times 10^6$ elements was used for the simulation to give a higher level of certainty. These results are shown in Figure 4. In addition, mesh refinement has been used around the blade's internal and external surfaces in order to increase the accuracy of the solution in fluid-solid interphases (i.e., flue gas-blade and cooling gas-blade interphases), thus ensuring that the mesh is more descriptive to the blade and provides a more accurate representation of its geometry. Moreover, the mesh quality (Table 6) is consistent with similar studies [32-34].

**Table 6.** Mesh properties.

| Property | Value |
|---|---|
| Elements maximum size (mm) | 0.01 |
| Number of elements | 8183531 |
| Growth rate | 1.2 |
| Defeature size (mm) | 0.00005 |
| Curvature minimum size (mm) | 0.0001 |
| Curvature normal angle (degree) | 12 |
| Skewness | 0.81 |
| Average Orthogonal Quality | 0.77 |
| Inflation transition ratio | 0.77 |
| Inflation number of layers | 5 |

The analysis performed in this paper is based on the $k$-$\varepsilon$ turbulence model shown in Equations (1-4) [35].

$$k = \frac{3}{2}(UI)^2 \tag{1}$$

$$\varepsilon = c_{\mu}^{\frac{3}{4}} k^{\frac{3}{2}} l^{-1} \tag{2}$$

$$I = 0.16 Re^{-\frac{1}{8}} \tag{3}$$

$$l = 0.07L \tag{4}$$

Where $I$ is the initial turbulence intensity [%], $U$ is the initial velocity magnitude, $l$ is the turbulence or eddy length scale, $c_{\mu}$is a specific $k-\varepsilon$ model parameter and $L$ is the characteristic length of interest.

ANSYS-CFX finds the numerical solution based on Navier-Stocks governing equations of mass, energy and momentum conservations, Equations (5-7) [36].

$$\frac{\partial \rho}{\partial t} + \nabla(\rho U) = 0 \tag{5}$$

$$\frac{\partial \rho U}{\partial t} + \nabla(\rho U \times U) = -\nabla p + \nabla \tau + S_M \tag{6}$$

$$\frac{\partial(\rho h_{tot})}{\partial t} - \frac{\partial p}{\partial t} + \nabla(\rho U h_{tot}) = \nabla(\lambda \nabla \mathrm{T}) + \nabla(\mathrm{U}.\tau) + \mathrm{U}.S_M + S_E \quad (7)$$

Where $\rho$, $t$, $U$, $\tau$, $p$, $S_M$, $h_{tot}$, $\lambda$, $S_E$ and T are the specific mass, time and the initial velocity, shear stress, Stagnation pressure, momentum source, total stagnation enthalpy, thermal conductivity, energy source, and temperature, respectively.

The velocity inlet boundary conditions (as specified in Figure 1 and Table 4) were set to a turbulence intensity of 10% as recommended by Butler et al. [35]. Residuals measure the local imbalance of a conserved variable in each control volume and the time rate of change of the conserved variable. In the iterative solution performed by ANSYS, residuals approach zero; however, the lower the residual target is, the more accurate the results are. Therefore, it was ensured in this study that the residual targets were as low as $1 \times 10^{-5}$. The results are shown in Figure 5.

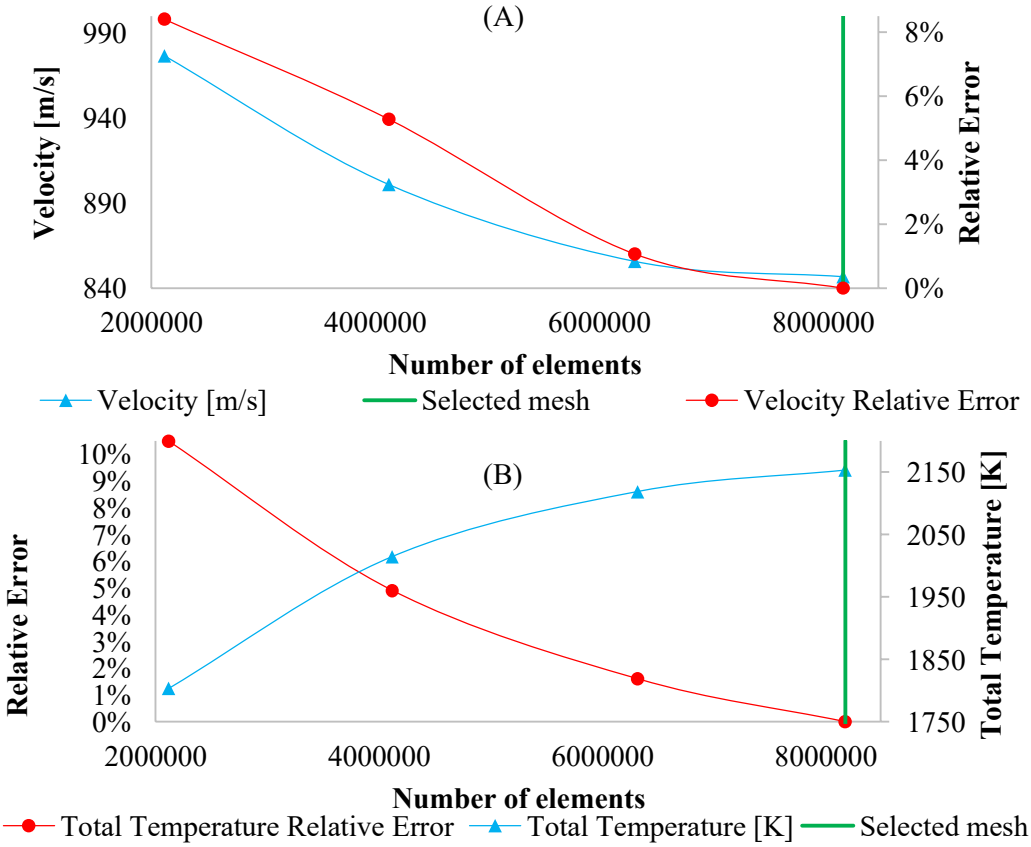


**Figure 3.** The mesh sensitivity analyses with respect to (A) the average velocity and (B) the average total temperature at the midspan plane.

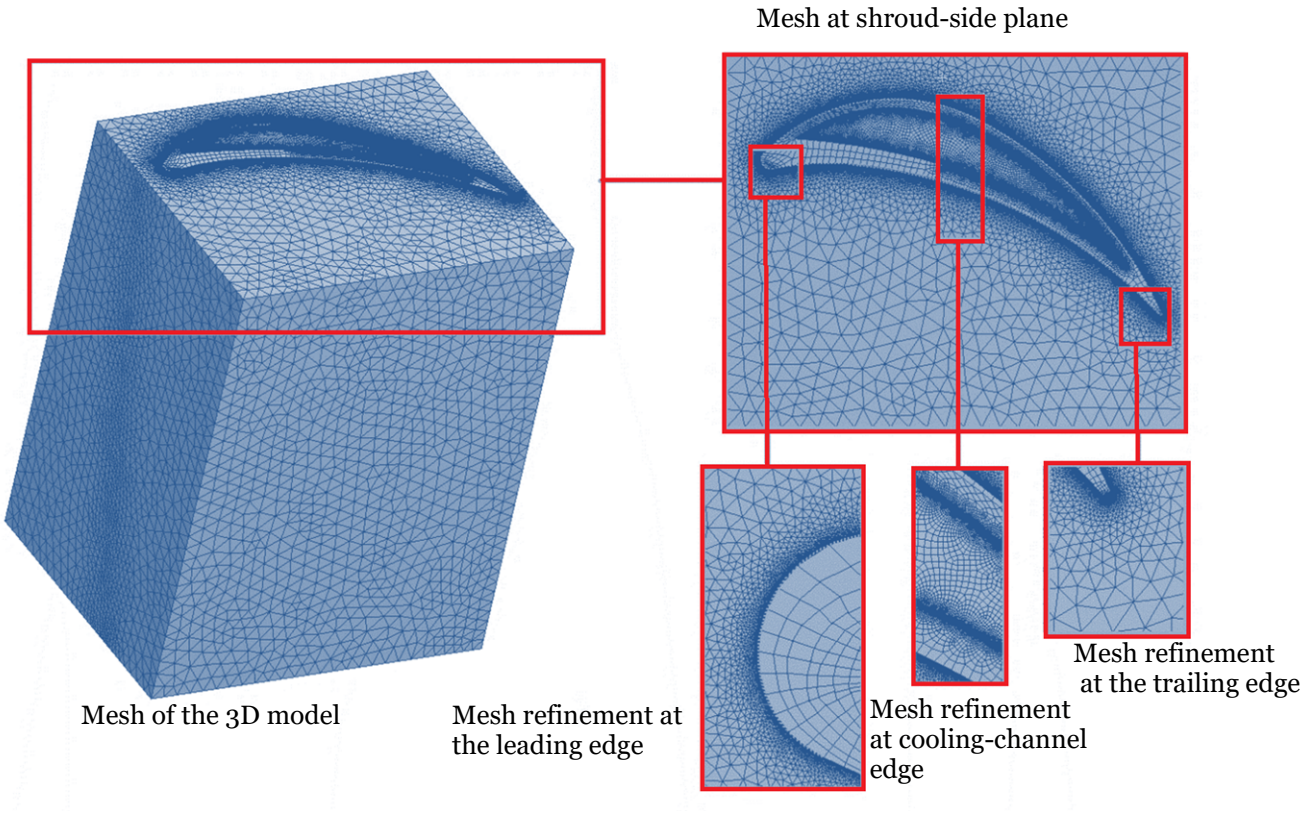


**Figure 4.** The CFX mesh of the model.

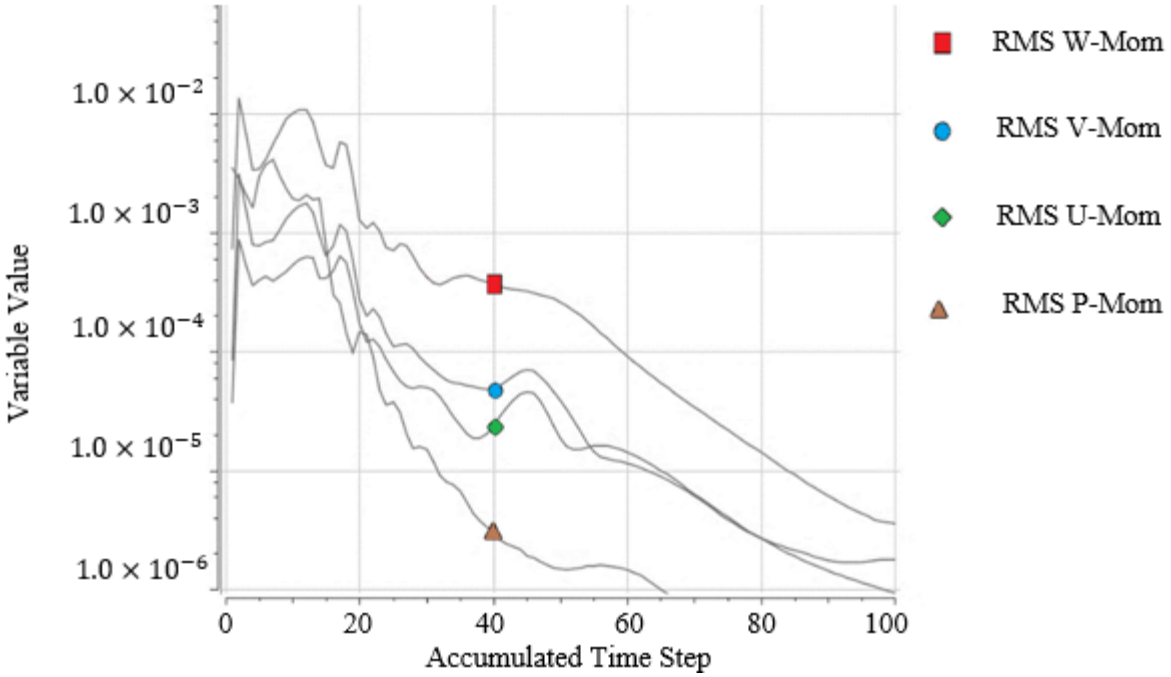


**Figure 5.** Convergence results.

## 3. RESULTS

Figure 6 shows the temperature contours of the turbine blade subjected to the flue gases of the $NH_3$-$H_2$/air and $CH_4$/air combustion at the stoichiometric conditions of $\Phi = 0.75$, 1, and 1.25, as specified in Tables 4 and 4. As discussed in section 2, the contours are displayed for the mid-span of the generic turbine blade. Shown in region A of Figure 6, there appears to be a small temperature

difference between the turbine blade leading edge and the inlet flow temperature (i.e. the blades temperature, also specified in Figure 9, was increased to approximately approach the flue gas temperatures in Table 4). This temperature difference was insignificant due to the cooling channel not effectively reducing the blade temperature at the mid-span plane. By correlating this finding to the heat flux contours in Figure 7, it should be noted that the highest level of heat flux is around the cold-gas inlet.

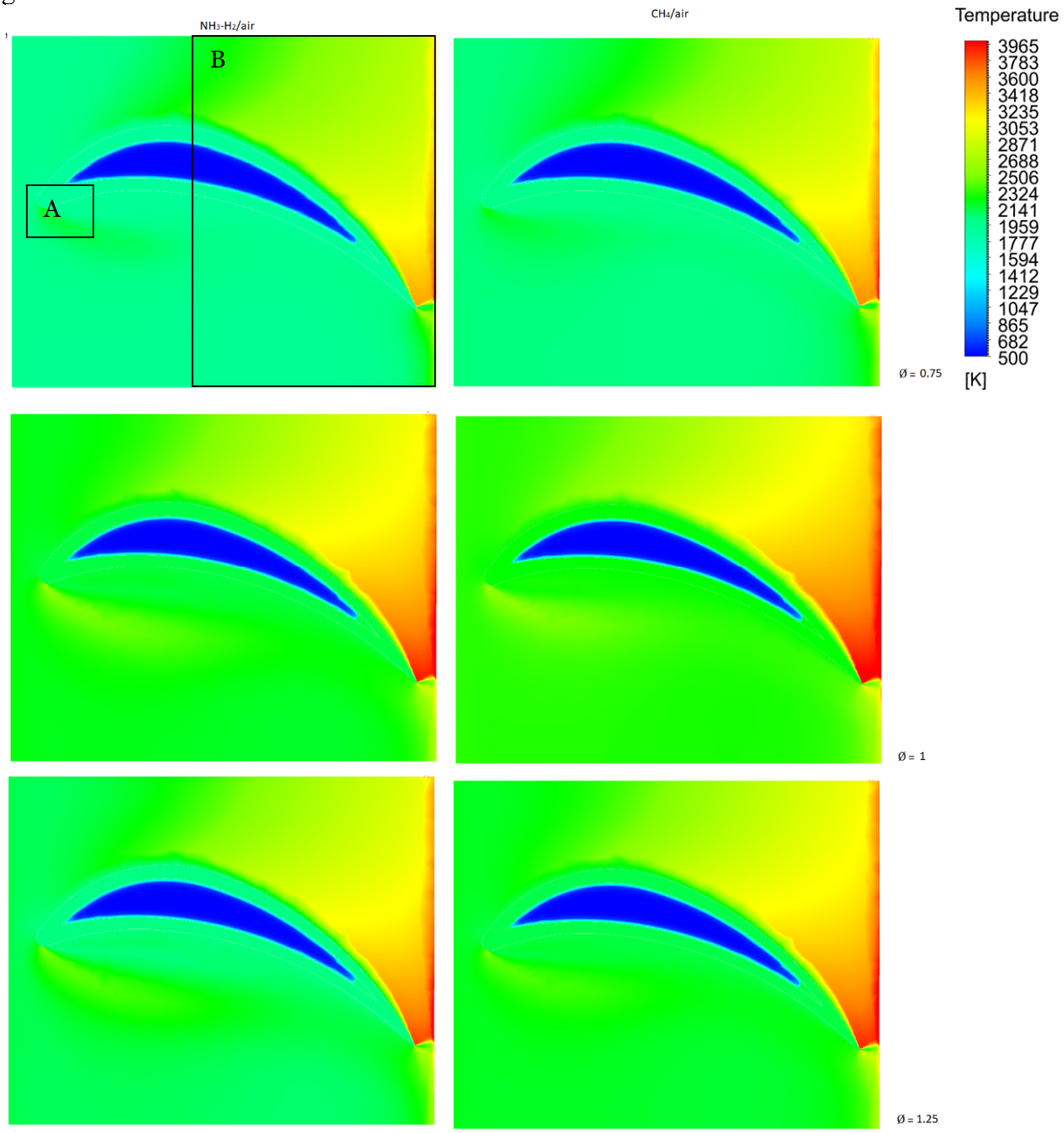


**Figure 6.** Temperature contours.

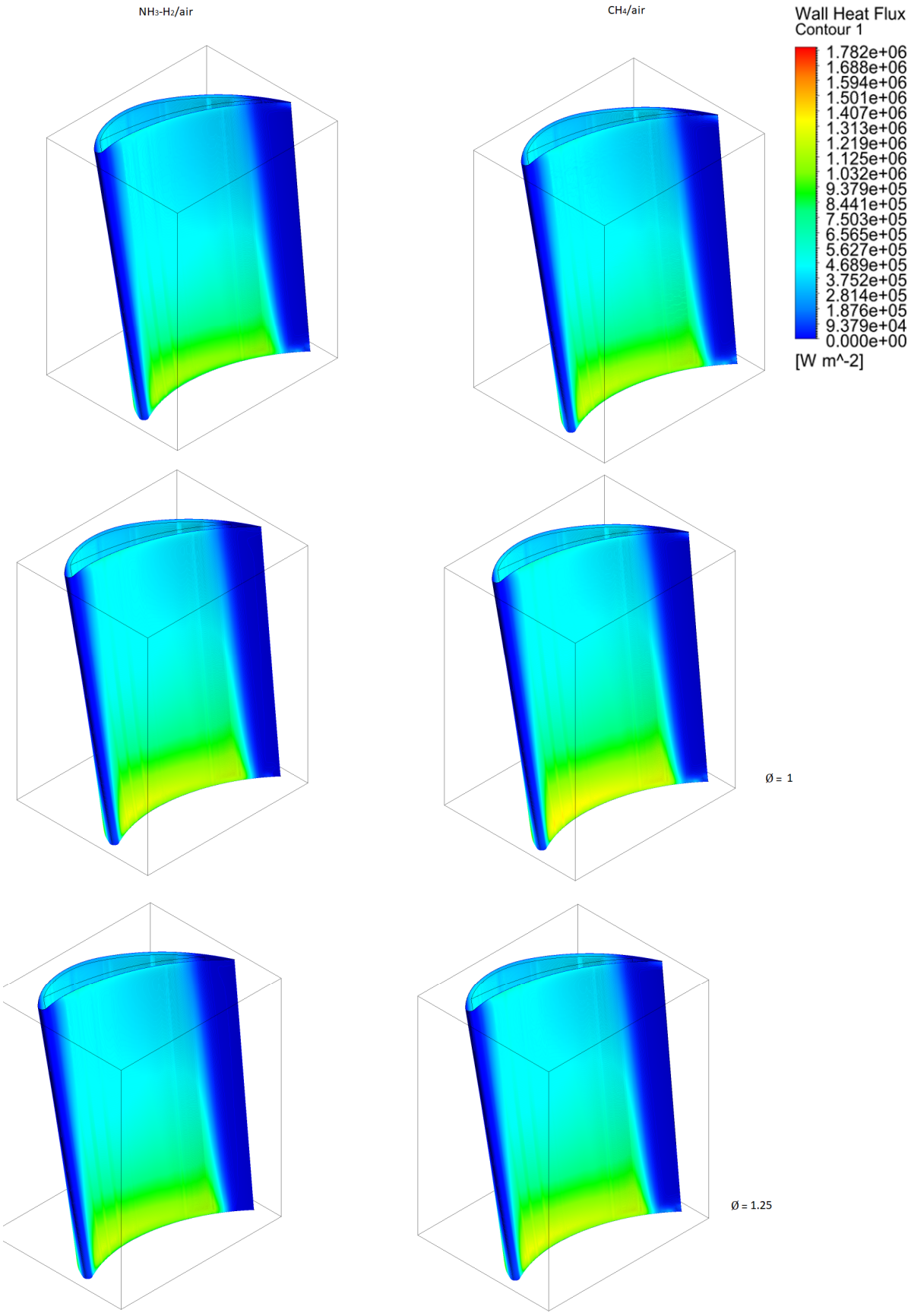


**Figure 7.** Heat Flux contours, the highest level of heat flux is around the cold-gas inlet and gradually decreases as the cold gas approaches its outlet

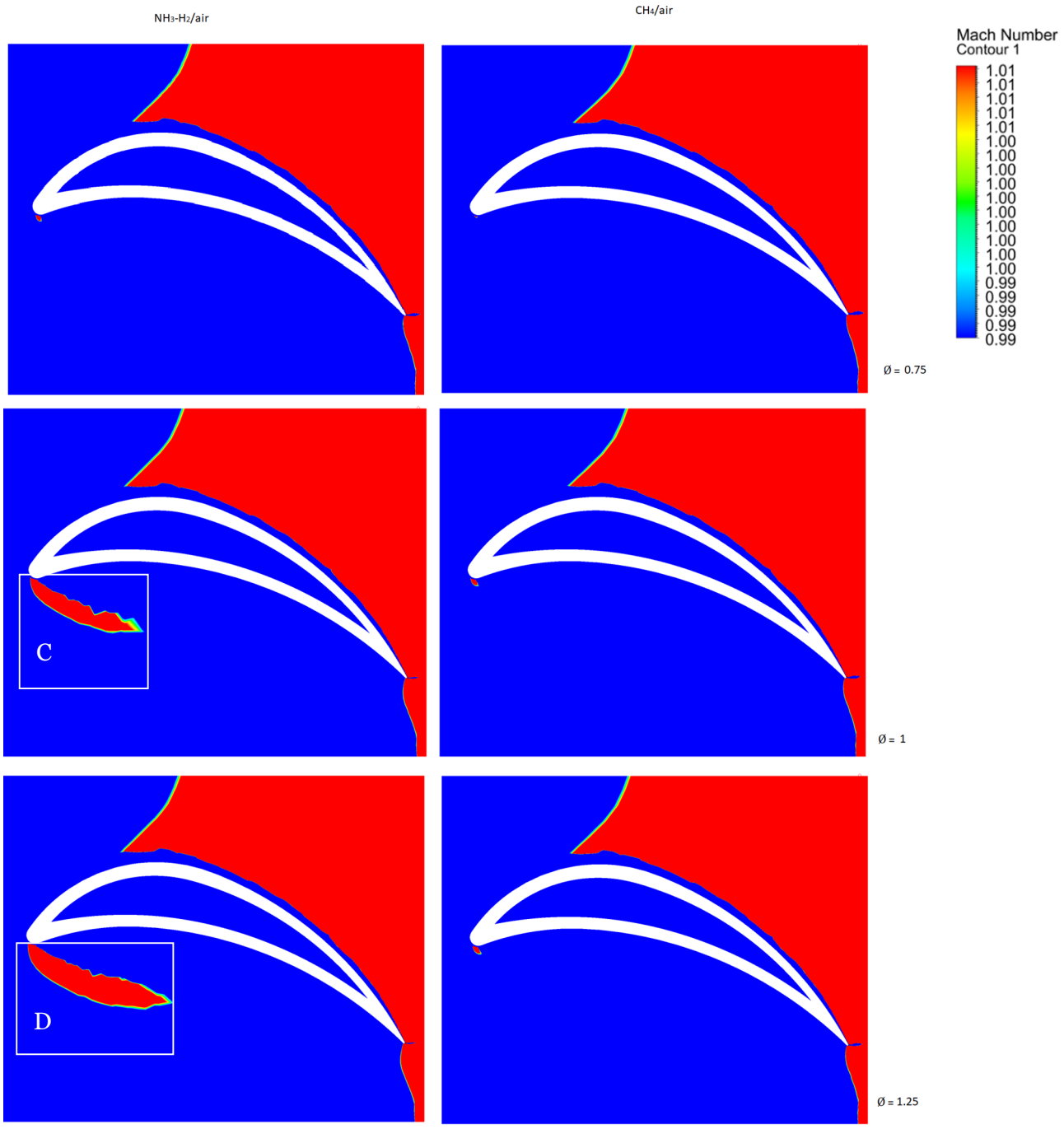


**Figure 8.** Shockwaves. As the equivalence ratio increases, a second shockwave is formed under the blade's lower surface (i.e., regions C and D).

The cold-gas temperature rapidly increases as it progresses through the cooling channel, due to the heat exchange between the hot flue gas and the cold channel gas, through the turbine blade's wall. Thus, the temperature difference between the two fluids reduces along the blade length, gradually decreasing the heat flux as the cold gas approaches its outlet. As the cold gas approaches the mid-span, its temperature increase prevents effective cooling in the blade walls.

As a result, as shown in the region A of Figure 6, the temperature difference between the leading edge and the turbine blade is insignificant. Thus, maintaining the turbine blade within acceptable temperature limits (~1644.15 K to 1813 K, depending on the alloy composition) would essentially require changing the cooling setups which are specified in Tables 4 and 5. This could be achieved by either changing the cold-gas inlet condition or composition (with a higher heat capacity, e.g. steam-based). Another potential solution was reported by Chen et al. [37], that of lowering the hydrogen content in the $NH_3$-$H_2$ fuel blend. This has a direct effect on reducing the flue gases temperature, however, this essentially means that the $NH_3$ content will be increased which could, as a result, increase the fuel $NO_x$ content in the flue gases. Therefore, a study characterizing the effects of varying the hydrogen content on $NO_x$ emissions and flue gas temperature, is recommended for future work. As shown in region B, the hot-gas temperature further increases as it approaches the blade's trailing edge. As shown in Figure 8, this temperature increase is directly attributed to the formation of a shockwave, as observed in a similar study [38], causing the post shock temperature to increase, as observed in a similar study [39] above 2150 K as shown in region B. By comparing the average and maximum temperatures of the turbine blade at the three combustion stoichiometric conditions of **Φ**=0.75, 1, and 1.25, as shown in Figure 9, it should be noted that the maximum temperature of the blade subjected to the $NH_3$-$H_2$/air combustion flue gases is lower than that of the blade subjected to the $CH_4$/air combustion flue gases through the entire tested equivalence ratio interval. In addition, as shown in Figure 9, the lowest blade maximum temperature is at **Φ**=0.75. However, at all stoichiometric conditions, the maximum blade temperature has exceeded the temperature limits of the used blade material (steel melting temperature is ~1813 K) because, as discussed previously, the cold gas has been found to be ineffective in significantly cooling down the blade across its entire span. The reason for choosing steel as the blade's material is to investigate whether this relatively less expensive material (compared to other costly materials with more advanced thermal properties) would sustain the thermal conditions of $NH_3$-$H_2$/air combustion flue gases. However, based on the results in Figure 9, a more advanced material is recommended for use. Moreover, as reported in the literature [3, 12-13], the equivalence ratio of 1.25 was recommended for $NH_3$-$H_2$/air combustion to maintain a relatively low level of emissions. However, this recommendation does not take into account the relatively high blade temperature or the need to consume the unburned fuel after the turbine. On the other hand, as reported by the reference [29], the equivalence ratio of 0.75 has maintained emissions approximately within those limits of the 1.25 equivalence ratio while showing a relatively higher cycle efficiency than $CH_4$/air combustion. In addition, as shown in Figure 9, the lowest blade temperature is found to be at the equivalence ratio of 0.75.

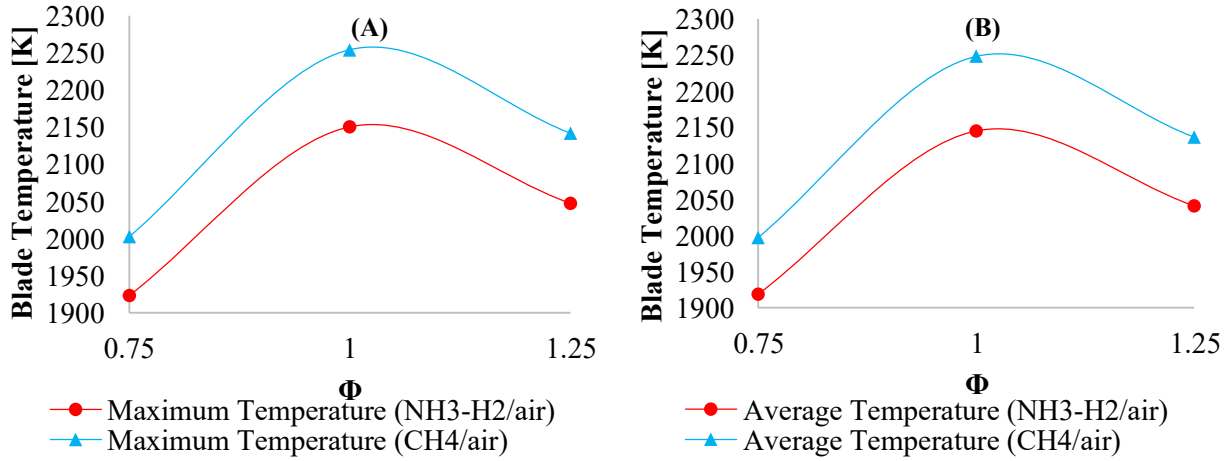


**Figure 9. (A)** Maximum and **(B)** average temperature of the turbine blade with respect to combustion stoichiometric conditions (of Φ=0.75, 1, and 1.25).

Figure 8 shows the Mach number contours. The contours have been plotted using a scale with a maximum allowable Mach number of 1 (shown in red), used as a threshold to indicate the shockwave location. As the flow over the blade's upper edge is transferred to the sonic and supersonic regions, oblique shockwaves are formed. Figures 8 and 10 show that the shockwave formation causes substantial total pressure losses as the flow passes through the shockwave (approximately from region E to region F, Figure 10).

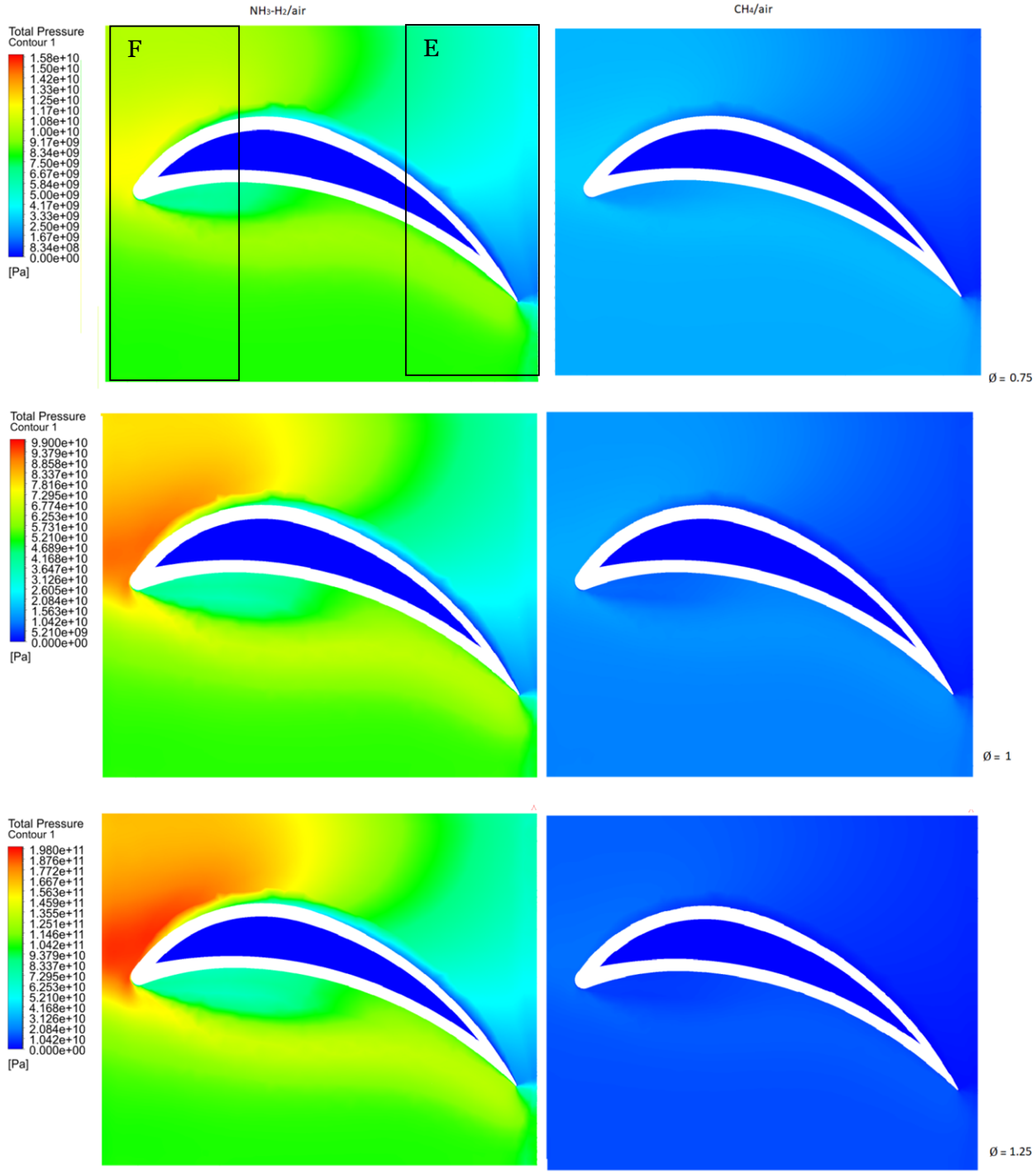


**Figure 10.**Total pressure contours.

As discussed in section 2, the contours are displayed for the mid-span plane. However, higher

pressure losses ($1 - P_{o_{outlet}}/P_{o_{inlet}}$) are expected near the end-walls of the blade (hub and shroud) because the formation of secondary flows becomes more significant [40]. In addition, as shown in Figure 8, as the equivalence ratio increases from 0.75 to 1.25, a second shockwave under the blade's lower edge is formed at the leading-edge surface (regions C and D). The formation of the second shockwave was more significant for the $NH_3$-$H_2$/air combustion flue gases compared to $CH_4$/air combustion, and the shockwave effect on pressure losses becomes more significant as the equivalence ratio increases to 1.25 (region D, Figure 8).

To quantify the pressure losses, the total losses across the computational domain are plotted in Figure 11. As shown in Figure 11, the pressure losses across the blade subjected to the flue gases of the $NH_3$-$H_2$/air combustion are higher than those on the blade subjected to the $CH_4$/air combustion flue gases throughout the entire tested stoichiometric interval ($\Phi$=0.75, 1 and 1.25). Moreover, as the flow of the $NH_3$-$H_2$/air flue gases forms a second shockwave under the blade's lower edge (when the equivalence ratio increases above 0.75), the pressure losses are further increased. The effect of increasing the equivalence ratio on increasing the pressure losses is more significant on the blade which is subjected to the flue gases of the $NH_3$-$H_2$/air combustion compared to $CH_4$/air (i.e., the pressure loss sensitivities towards the equivalence ratio ($\partial(1 - P_{o_{outlet}}/P_{o_{inlet}})/\partial\Phi$) are approximately 0.125 and 0.118 for the $NH_3$-$H_2$/air and $CH_4$/air combustion, respectively). Increased pressure losses create pressure drag caused by the pressure differential between the front and rear surfaces of the blade [41], as shown in Figure 11. As the equivalence ratio increases from 0.75 to 1.25, the velocity of the combustion flue gases increases from 451.7 m/s to 569.7 m/s, respectively (Table 4), thus, the flow over the blade become faster than the local sound speed, and there is an abrupt decrease in the flow area. This is an irreversible flow process as the local entropy increases. Shock waves are generated and become more significant as the combustion flue gas velocity increase (i.e., at an equivalence ratio of 1.25). Because the flow is non-isentropic, the total pressure downstream of the shock is always less than the total pressure upstream of the shock.

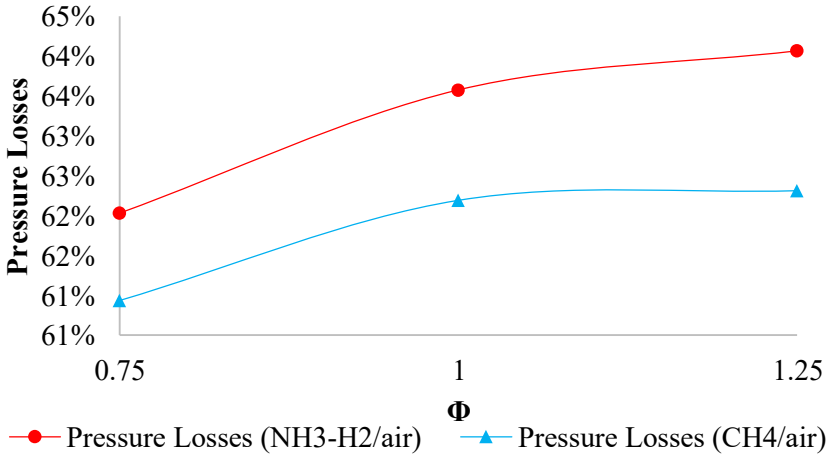


**Figure 11.** Total pressure losses across the turbine blade.

Figure 12 shows the Mach number contours of the turbine blade subjected to the flue gases of the $NH_3$-$H_2$/air and $CH_4$/air combustion at the stoichiometric conditions of $\Phi$=0.75, 1, and 1.25, as specified in Tables 4 and 5. Due to the passage area increase in region G, the Mach number increased. The opposite effect was observed in the region I as the passage area decreased. As regions I and G have two opposing effects on the overall average outlet Mach number ($M_{out}$), it is essential to plot the overall average Mach numbers over the flow inlet and outlet. Figure 13 shows that the turbine blade outlet Mach number ($M_{out}$ ) increases compared to the overall average inlet Mach number ($M_{in}$) at all stoichiometric conditions using both the $NH_3$-$H_2$ and $CH_4$ fuels. As shown in Figure 13.B, the blade's effect on increasing $M_{out}$ compared to $M_{in}$ has been quantified by plotting

the $M_{out}$ to $M_{in}$ ratio ($M_{out}/M_{in}$).
Within the tested equivalence ratios Φ=0.75, 1, and 1.25, the blade's capability of increasing $M_{out}$ is higher for the $CH_4$/air flue gases compared to $NH_3$-$H_2$/air. Moreover, as the $NH_3$-$H_2$/air combustion equivalence ratio increases from 0.75 to 1.25, the blade's capability of increasing $M_{out}$ compared to $M_{in}$ drastically decreases (as $M_{out}/M_{in}$ decreases). This is attributed to the formation of the secondary shockwave under the blade's lower edge at the leading-edge surface [38] (regions C and D, Figure 8), which causes the local Mach number after the shockwave to reduce, thus affecting the overall average Mach number over the outlet plane at regions H, J and K approximately dropping to a near-zero level.

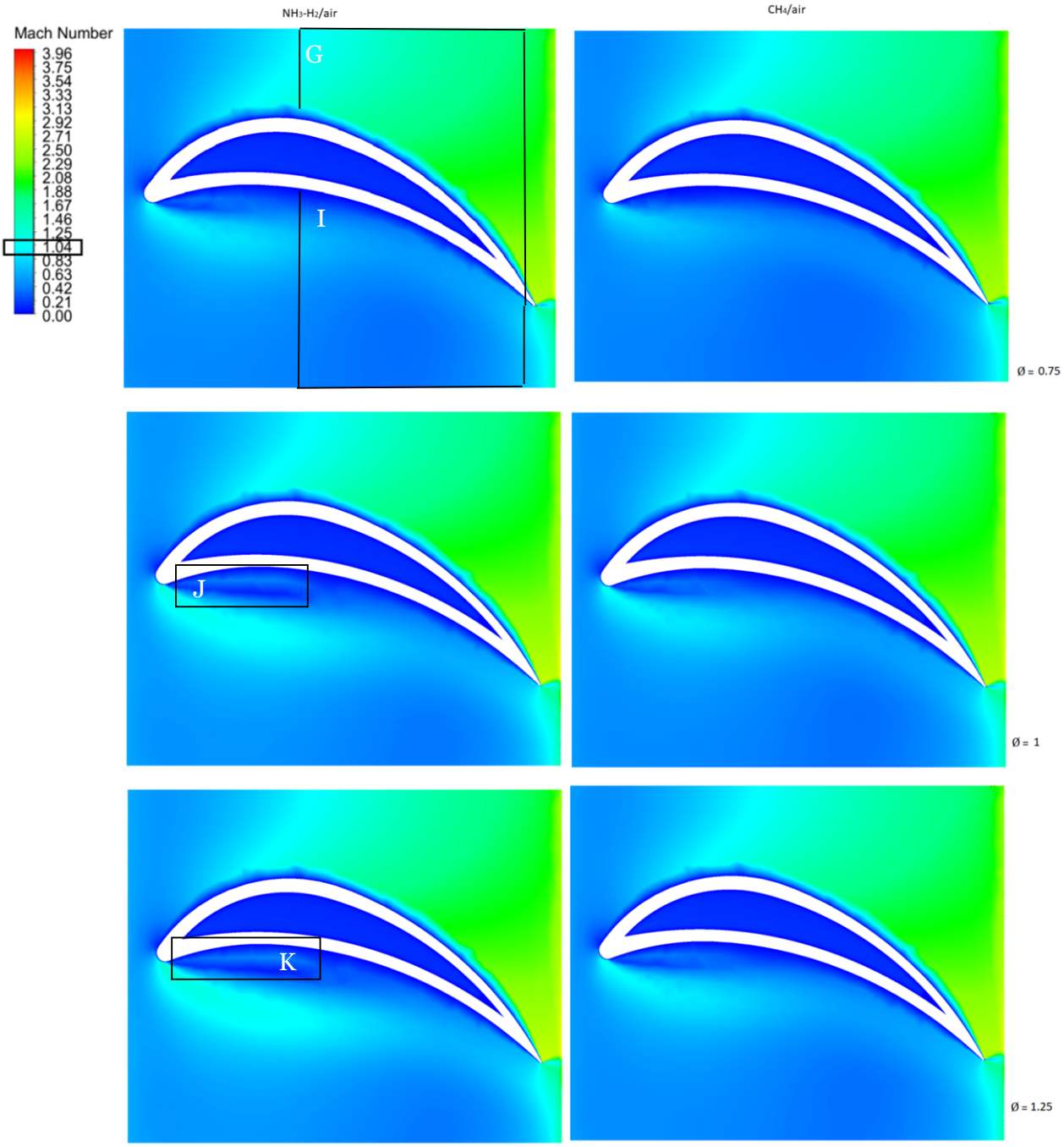


**Figure 12.** Mach number contours.

The formation of the second shockwave becomes more significant as the equivalence ratio increases causing the near-zero-Mach-number regions to expand (regions H, J and K), which as a result, reduces the blade's capability of increasing the average overall outlet Mach number compared to the inlet ($M_{out}/M_{in}$).
The Mach number approximately dropped to zero at regions H, J, and K as the flow separation occurs at those regions (H, J and K as the flow slows down and increases pressure after passing through a widening passage [42]).

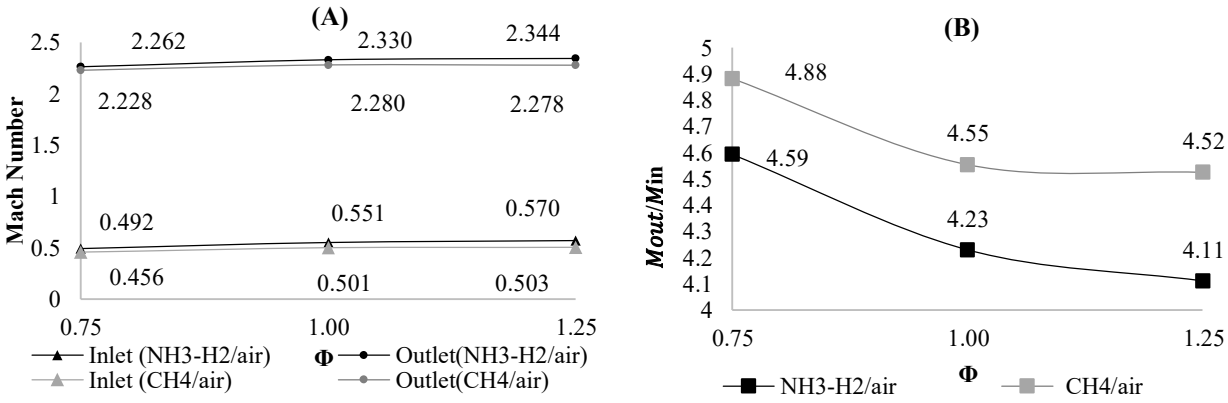


**Figure 13. (A)** Average inlet Mach number ($M_{in}$) and outlet Mach numbers ($M_{out}$) **(B)** the $\mathrm{M_{out}}$ to$\mathrm{M_{in}}$ ratio ($\mathrm{M_{out}/M_{in}}$).

A combination of the streamline and pressure gradient plots are shown in Figure 14. These plots have been generated to highlight the flow separation regions where local zero pressure gradients and vortices are formed, highlighting the reduction in the Mach number, which as a result led to a reduction of the blade's capability of increasing $M_{out}/M_{in}$.

Also shown in Figure 14, the pressure gradient contours have been plotted using a scale with a maximum allowable pressure gradient of 0, used as a threshold to locate the flow separation (its location appears when the cooler scale, which is assigned to the maximum permissible pressure gradient of 0 (yellow), appears). Figure 14 also illustrates, the $NH_3$-$H_2$/air combustion flue gases' pressure gradient ($\partial P/\partial x$) transferred from the positive interval to the negative interval. Flow separation effectively occurs when the pressure gradient hits the zero limit ($\partial P/\partial x=0$, highlighted in yellow in Figure 14). This occurs at the leading and trailing edges on both of the upper and lower surfaces (regions L and M). For the blade subjected to the $CH_4$/air combustion flue gases, the separation pattern over the blade was approximately similar to the $NH_3$-$H_2$/air combustion flue gases. However, while the separation pattern near the trailing edge of the $CH_4$/air combustion flue gases was similar to NH3-$H_2$/air combustion flue gases (Regions Q and M), the separation that occurred near the leading edge was less significant compared to the $NH_3$-$H_2$/air combustion flue gases (Regions L and O). This essentially means that for a given geometry, the flow separation is more significant using the $NH_3$-$H_2$ fuel. This can be attributed to the kinematic viscosity differences between the $CH_4$ and $NH_3$-$H_2$ fuels. Kinematic viscosity for the $NH_3$-$H_2$ fuel is higher compared to the $CH_4$ fuel (i.e., $2.06 \times 10^{-5}$ $m^2/s$ and $1.75\times 10^{-5}$ $m^2/s$, respectively) which causes the boundary layer to possess a higher viscous force and fluid inertia, inducing an increase to higher levels of separation.

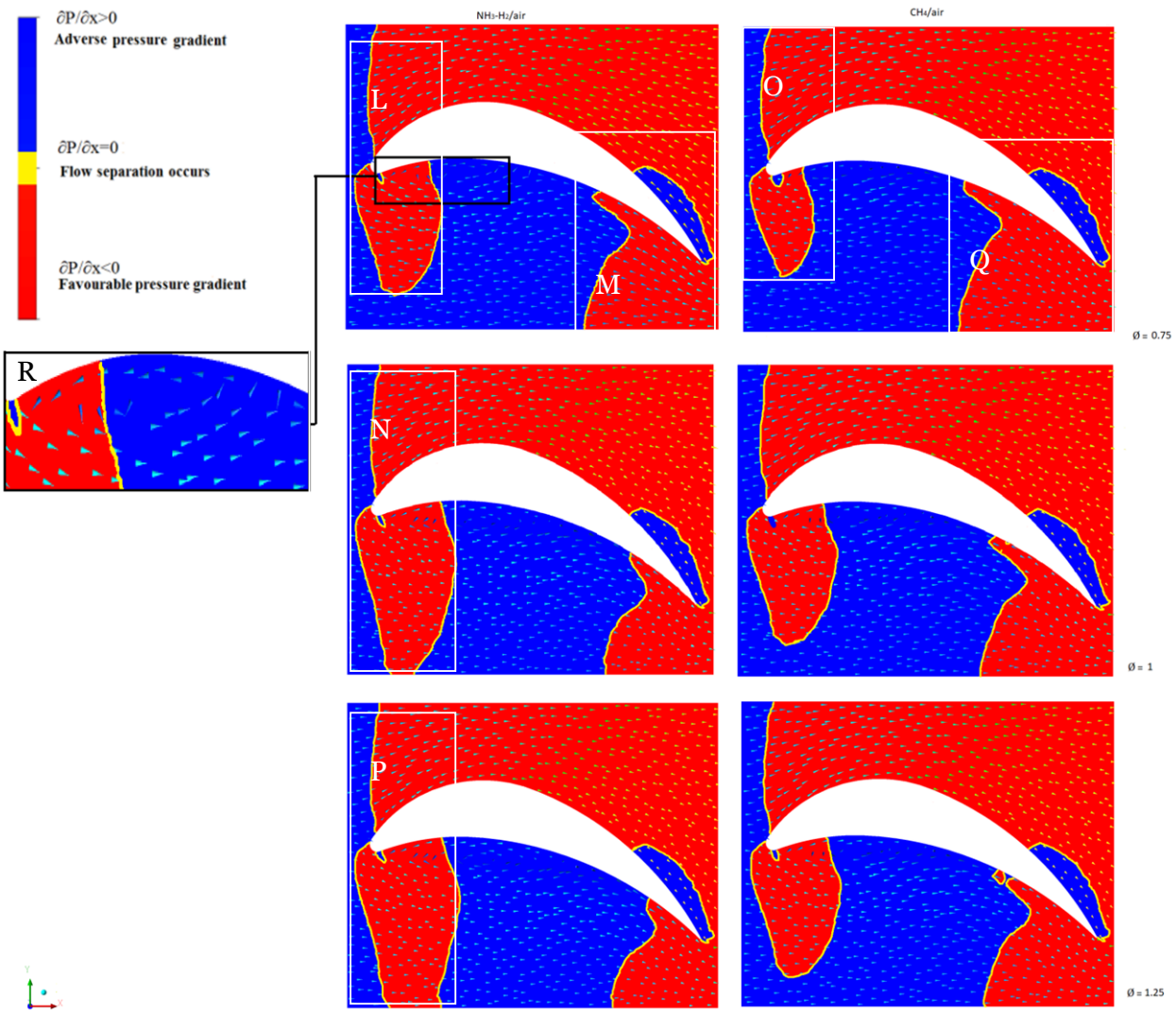


**Figure 14.** Pressure gradient contour and velocity streamline.

As the equivalence ratio increases from 0.75 to 1.25, the flow separation near the trailing edge remains practically unaffected. However, the separation near the leading edge at the blade's lower edge becomes more significant (regions L, N and P), causing a circulation zone under the blade's lower surface (region R). The recirculation in this region creates high turbulence energy in the form of eddies and vortices, as shown in Figure 15, causing vibrations in machinery blading [43]. Figure 15 also shows the $NH_3$-$H_2$/air combustion flue gases exhibiting higher levels of turbulent kinetic energy under the blade's lower surface when compared to the $CH_4$/air combustion flue gases, due to the higher levels of fluid shear and flow circulation. As the equivalence ratio increases from 0.75 to 1.25, the turbulent kinetic energy is further increased (Regions S, T, and V). The equivalence ratio effect on the turbulent kinetic energy is quantified over the mid-span plane, as shown in Figure 16. The significant kinetic energy loss [44] demonstrates that it is essential to operate the gas turbine under the operation condition which minimizes turbulent energy (i.e., within the tested equivalence ratio, the minimum turbulent energy over the blade is found to be at 0.75). As the equivalence ratio increases from 0.75 to 1.25, the velocity of the combustion flue gases increases from 451.7 m/s to 569.7 m/s, respectively (Table 4), and the turbulent kinetic energy increases correspondingly because it is directly proportional to the square of the gas flow velocity (i.e., $k \propto U^2$), see Equation 1.

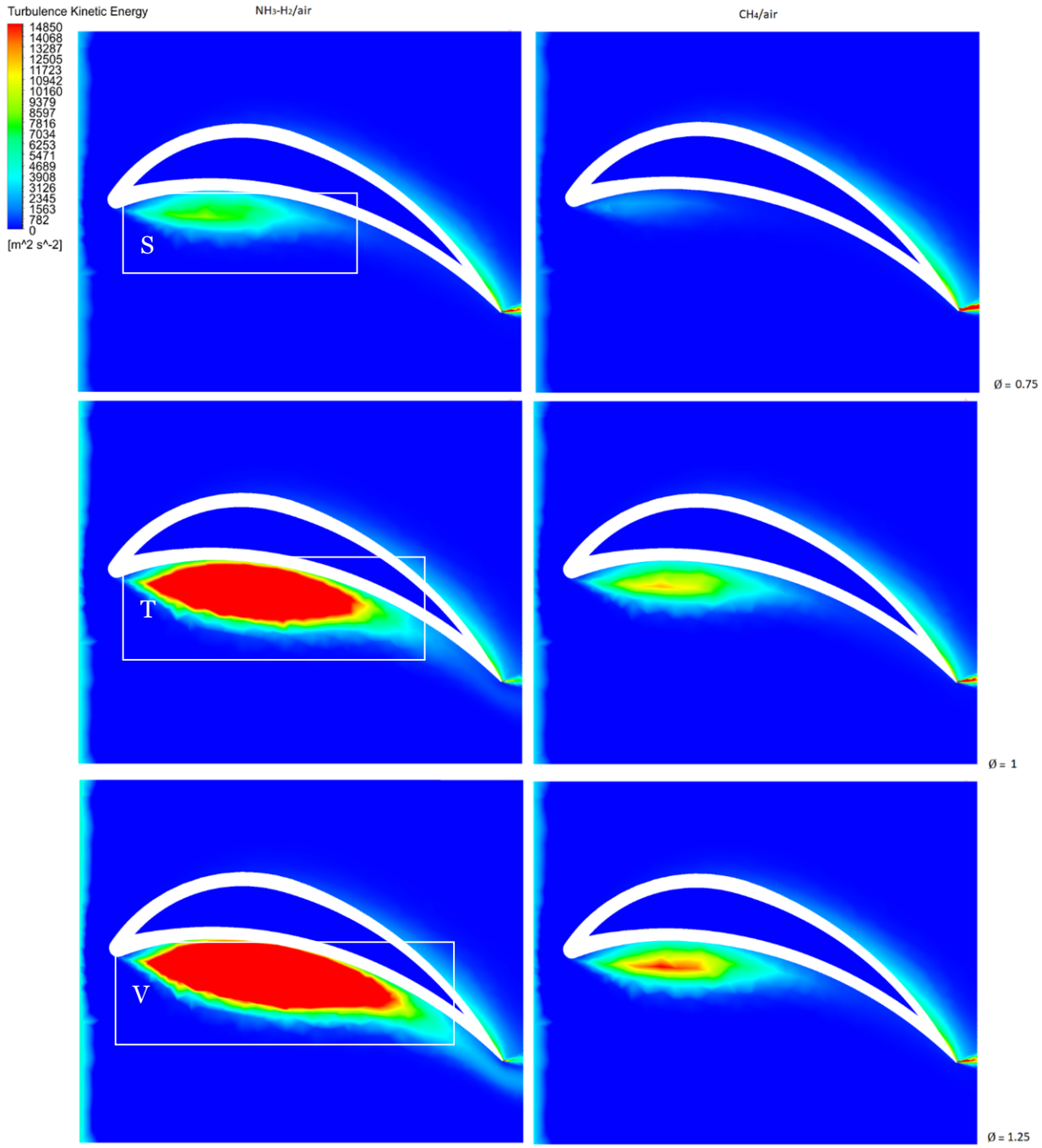


**Figure 15.** Turbulent kinetic energy contour.

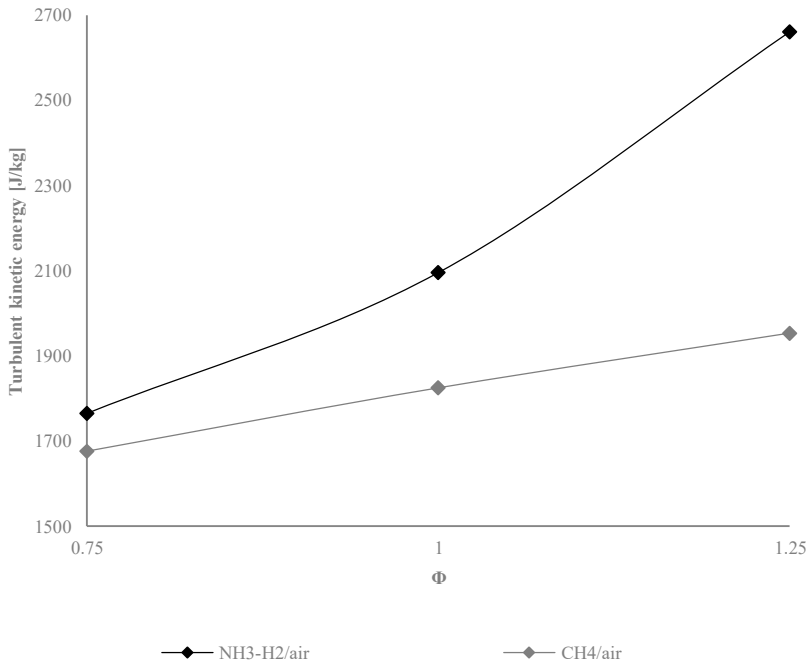


**Figure 16.** Average Turbulent kinetic energy over the mid-span.

## 4. DISCUSSION

Considering the tested parameters in this study (the maximum temperature of the turbine blade, the pressure losses, the blade's capability of increasing $M_{out}$ and turbulent kinetic energy), it can be concluded that operating an $NH_3$-$H_2$/air gas turbine is ideally conducted with an equivalence ratio of 0.75 for the following reasons;

1. The maximum temperature of the blade subjected to the $NH_3$-$H_2$/air combustion flue gases was found to be at its highest levels at an equivalence ratio of 1 (2150.5 K) and the lowest at an equivalence ratio of 0.75 (1923.6 K). If minimizing the blade's maximum temperature is of primary concern, taking into account the chosen material, operating gas turbines at an equivalence ratio of 0.75 is recommended. Alternatively, implementing more advanced cooling techniques would be required.
2. Operating the $NH_3$-$H_2$/air gas turbine at an equivalence ratio of 1.25 essentially imposes the highest levels of pressure losses over the turbine blade compared to other stoichiometric conditions ( $1 - P_{o_{outlet}}/P_{o_{inlet}} = 0.64$). The minimum pressure losses were found to be at an equivalence ratio of 0.75 ($1 - P_{o_{outlet}}/P_{o_{inlet}} = 0.62$) making this more efficient. However, in both conditions, the pressure losses over the turbine blade due to $CH_4$/air combustion were found to be marginally lower than those of the $NH_3$-$H_2$/air combustion (i.e., 0.623 and 0.61 at the equivalence ratios of 1.25 and 0.75, respectively), which seems to be characteristic of the $NH_3$-$H_2$ fuel blend.

   As the equivalence ratio increases, the blade's ability to increase the outlet Mach number ($M_{out}/M_{in}$) for the $NH_3$-$H_2$/air combustion, drops by approximately 12% (i.e., 4.6 and 4.11 at the equivalence ratios of 0.75 and 1.25, respectively). The same effect was observed on the $CH_4$/air combustion, however, $M_{out}/M_{in}$ was less sensitive to the equivalence ratio increase as the reduction was only 8% (i.e., 4.88 and 4.52 for the equivalence ratios of 0.75 and 1.25, respectively).
3. To minimize the fluid energy losses associated with turbulent kinetic energy, operating the

$NH_3$-$H_2$/air gas turbine at an equivalence ratio of 1.25 must be avoided as it imposes a 50% increase in turbulent kinetic energy compared to the equivalence ratio of 0.75. In addition, Fuel-lean combustion (0.75) also increases combustion efficiency as reported by [29].

Table 7 shows the outcome of this study comparatively for the $NH_3$-$H_2$/air and $CH_4$/air combustion at the three equivalence ratios. These results highlight the recommended operation condition, the condition to be avoided and the increase or reduction ratio ($V_r/V_{TBA} - 1$) of each parameter's value at its recommended condition ($V_r$) to its value at the To-Be-Avoided conditions ($V_{TBA}$).

**Table 7**. The recommended and the To-Be-Avoided equivalence ratios with respect to the studied parameters (the maximum temperature of the turbine blade, the pressure losses, the blade's capability of increasing $M_{out}$ and turbulent kinetic energy).

| Parameter (V) | Combustion type | Φ | | | Recommended equivalence ratio $\Phi_r$ | To-Be-Avoided equivalence ratio $\Phi_{TBA}$ | $\frac{V_{TBA}}{V_r} - 1$ [%] |
|---|---|---|---|---|---|---|---|
| | | 0.75 | 1 | 1.25 | | | |
| The maximum temperature of the blade [K] | $NH_3$-$H_2$/air | 1923.58 | 2150.47 | 2047.3 | 0.75 | 1 | 11.8 |
| | CH4/air | 2002.54 | 2254.08 | 2141.9 | 0.75 | 1 | 12.6 |
| Total pressure loss | $NH_3$-$H_2$/air | 0.6203 | 0.6357 | 0.6407 | 0.75 | 1.25 | 3.29 |
| | CH4/air | 0.60934 | 0.62189 | 0.62311 | 0.75 | 1.25 | 2.26 |
| Average turbulent kinetic energy [J/kg] | $NH_3$-$H_2$/air | 1764.9 | 2095.28 | 2661.12 | 0.75 | 1.25 | 50.8 |
| | CH4/air | 1675.6 | 1824.73 | 1953.17 | 0.75 | 1.25 | 16.6 |
| Parameter | Combustion type | Φ | | | Recommended Φ | To-Be-Avoided Φ | $\frac{V_r}{V_{TBA}} - 1$ [%] |
| | | 0.75 | 1 | 1.25 | | | |
| $M_{out}/M_{in}$ | $NH_3$-$H_2$/air | 4.6 | 4.23 | 4.11 | 0.75 | 1.25 | 11.9 |
| | CH4/air | 4.88 | 4.55 | 4.52 | 0.75 | 1.25 | 7.9 |

## 5. CONCLUSIONS

The $NH_3$-$H_2$ fuel blend offers a novel solution to eliminate carbon emissions. However, adopting this fuel blend as an alternative to the $CH_4$ fuel required knowledge of the flue gas dynamics on the turbine blade, an aspect that has not been carefully considered in the $NH_3$-$H_2$ literature to date. This paper investigated the gas dynamics using CFD analysis and identified differing flow features to $CH_4$ fuel combustion. These differences included higher pressure losses, increased fluid energy losses associated with high turbulent kinetic energy, and low capability of increasing the outlet Mach number compared to $CH_4$-air. Specifically, the results of the study determined that, from a set of three evaluated equivalence ratios (0.75, 1.00, and 1.25), the leanest mixture of 0.75 was found to best reduce pressure losses and viscous energy losses, while also minimising the blade's operational temperature.

The maximum temperature of the blade subjected to the $NH_3$-$H_2$/air combustion flue gas at the equivalence ratio of 0.75 is reduced by approximately 123 K compared to the equivalence ratio of 1.25 and by 226 K compared to the equivalence ratio of 1.00. This counts for 6% and 11.8% temperature reduction ratios compared to the equivalence ratios of 1.25 and 1.00, respectively.

In addition, operating the $NH_3$-$H_2$/air gas turbine at the equivalence ratio of 0.75 reduces the total pressure losses over the blade by approximately 3.3% and 2.5% compared to the equivalence ratios of 1.25 and 1.00, respectively. Moreover, at the equivalence ratio of 0.75, the average turbulent kinetic energy is significantly reduced by approximately 51% and 19% compared to the equivalence ratios of 1.25 and 1.00, respectively.

The equivalence ratio of 1.25 for the $NH_3$-$H_2$ fuel has been proposed in the literature solely due to its emission performance. The $NH_3$-$H_2$ fuel blend remains a promising alternative fuel candidate. However, the results of this study demonstrate that implementing the $NH_3$-$H_2$ fuel needs further consideration of the gas dynamics and requires a more quantitative study to determine the conditions which would enhance the possibility of promoting this fuel for widespread use, without imposing major amendments on existing gas turbines. This essentially requires performing component matching analysis of $NH_3$-$H_2$ gas turbines that could be verified through performing experimental analysis on $NH_3$-$H_2$ gas turbine prototypes. In addition, considering the computational complexity and the recommendations in the literature, it is crucial to highlight that this study was limited to three stoichiometric conditions (i.e., $\Phi = 0.75$, $\Phi = 1.00$ and $\Phi = 1.25$). Therefore, as future work, it is recommended investigate more stoichiometric conditions. In addition, it is recommended to propose an economically sustainable process that is calibrated to provide a continuous supply of the 70 % $NH_3$ - 30 % $H_2$ (vol. %) fuel blend. Such processes could be developed and evaluated in process simulation programs (such as ASPEN PLUS/HYSIS). Finally, $NO_x$ mitigating approaches shall be further investigated for this blend and the aspect of $NO_x$ capturing shall be carefully considered.

## NOMENCLATURE

| | |
|---|---|
| k | Turbulent Kinetic Energy (J/kg) |
| U | Initial velocity magnitude (m/s) |
| I | Initial turbulence intensity |
| l | Turbulence or eddy length scale |
| $\rho$ | Specific Mass (kg/m³) |
| $t$ | Time (s) |
| $\tau$ | Shear stress (Pa) |
| $p$ | Stagnation pressure(Pa) |
| $S_M$ | Momentum source (N.m) |
| $h_{tot}$ | Total stagnation enthalpy (J/kg) |
| $\lambda$ | Thermal conductivity (W/m.K) |
| $S_E$ | Energy source (J) |
| T | Temperature (K) |
| $c_\mu$ | k–ε model parameter |
| $\dot{m}_{a,p}$ | Primary Airflow rate [kg/s] |
| $\dot{m}_f$ | Fuel flow rate [kg/s] |
| $P_{02}/P_{01}$ | Compressor pressure ratio |
| $T_{03}$ | Combustion outlet temperature [K] |
| $T_{03.t}$ | Turbine inlet temperature [K] |
| $\varepsilon$ | Turbulent Kinetic Energy Dissipation (J/kg) |
| Re | Reynolds number |
| $T_{01}$ | Compressor inlet temperature [K] |
| $T_{02}$ | Compressor outlet temperature [K] |
| $P_{01}$ | Compressor inlet pressure [bar] |

| | |
|---|---|
| $P_{02}$ | Compressor outlet pressure [bar] |
| $M_{in}$ | Inlet Mach number |
| $M_{out}$ | Outlet Mach number |
| $\Phi$ | Equivalence ratio |
| SST | Shear Stress Transport |
| SSTCC | Shear Stress Transport with Curvature Correction |
| RSM | Reynolds-Stress Models |


## FUNDING

This publication was made possible by NPRP 12 grant # (NPRP12C-0821-190017) from the Qatar National Research Fund (a member of the Qatar Foundation). The findings herein reflect the work and are solely the responsibility of the authors. Open Access funding provided by the Qatar National Library.


## REFERENCES


[1] Bancalari, Ed, Pedy Chan, and Ihor S. Diakunchak. "Advanced hydrogen turbine development." In 23rd International Pittsburgh Coal Conference, Pittsburgh, Pennsylvania. 2006.

[2] Anderson, Reed. "GE Perspectives–Advanced IGCC/Hydrogen Gas Turbine Development." In 2010 University Turbine Systems Research Workshop, State College, PA, http://www. netl. doe. gov/publications/proceedings/10/utsr/presentations/tuesday/Anderson. Pdf. 2010.

[3] Valera-Medina, Agustin, D. G. Pugh, P. Marsh, G. Bulat, and Philip Bowen. "Preliminary study on lean premixed combustion of ammonia-hydrogen for swirling gas turbine combustors." International Journal of Hydrogen Energy 42, no. 38 (2017): 24495-24503.

[4] Syed Mashruk, Hua Xiao and Agustin Valera-Medina. "Rich-Quench-Lean model comparison for the clean use of humidified ammonia/hydrogen combustion systems." International Journal of Hydrogen Energy 46, no. 5 (2021): 4472-4484.

[5] [Online; accessed 03-March-2021], https://power.mhi.com/news/20210301. html; 2021.

[6] Iki Norihiko, Kurata Osamu, Matsunuma Takayuki, Inoue Takahiro, Tsujimura Taku, Furutani Hirohide, Kobayashi Hideaki, Hayakawa Akihiro, Arakawa Yoshiyuki, Ichikawa Akinori. Micro gas turbine firing ammonia. In: Turbo expo: power for land, sea, and air, vol. 49866. American Society of Mechanical Engineers; 2016, V008T23A018.

[7] Okafor Ekenechukwu C, Somarathne KDKunkuma A, Hayakawa Akihiro, Kudo Taku, Kurata Osamu, Iki Norihiko, Kobayashi Hideaki. Towards the development of an efficient low-nox ammonia combustor for a micro gas turbine. Proc Combust Inst 2019;37(4):4597e606.

[8] Pashchenko, Dmitry, Ravil Mustafin, and Igor Karpilov. "Ammonia-fired chemically recuperated gas turbine: Thermodynamic analysis of cycle and recuperation system." Energy 252 (2022): 124081.

[9] Verkhivker Gregoriy, Kravchenko Vladimir. The use of chemical recuperation of heat in a power plant. Energy 2004;29(3):379e88.

[10] Sadeghi Mohsen, Chitsaz Ata, Marivani Parisa, Yari Mortaza, Mahmoudi SMS. Effects of thermophysical and thermochemical recuperation on the performance of combined gas turbine and organic rankine cycle power generation system: thermoeconomic comparison and multi-objective optimization. Energy 2020;210:118551.

[11] Kobayashi, Hideaki, Akihiro Hayakawa, KD Kunkuma A. Somarathne, and Ekenechukwu C. Okafor. "Science and technology of ammonia combustion." Proceedings of the Combustion Institute 37, no. 1 (2019): 109-133.

[12] Shrestha, Krishna Prasad, Charles Lhuillier, Amanda Alves Barbosa, Pierre Brequigny, Francesco Contino, Christine Mounaïm-Rousselle, Lars Seidel, and Fabian Mauss. "An experimental and modeling study of ammonia with enriched oxygen content and ammonia/hydrogen laminar flame speed at elevated pressure and temperature." Proceedings of the Combustion Institute 38, no. 2 (2021): 2163-2174.

[13] Hua Xiao, Michael Howard, Agustin Valera-Medina, Stephen Dooley, and Philip J. Bowen. "Study on reduced chemical mechanisms of ammonia/methane combustion under gas turbine conditions." Energy & Fuels 30, no. 10 (2016): 8701

[14] Town, D. Straub, J. Black, K.A. Thole, T.I. Shih, State-of-the-Art Cooling Technology for a Turbine Rotor Blade, ASME. J. Turbomach. 140 (7) (2018) 071007, doi:10.1115/1.4039942.

[15] J. Han, S. Dutta, Recent Developments in Turbine Blade Internal Cooling, Ann. N. Y. Acad. Sci. 934 (2001) 162–178, doi:10.1111/j.1749-6632.2001.tb05850.

[16] D.J. Doorly, M.L.G. Oldfield, Simulation of the Effects of Shock Wave Passing on a Turbine Rotor Blade, ASME,

J. Eng. Gas Turbines Power. 107 (4) (1985) 998–1006, doi:10.1115/1.3239847.
[17] K. Funazaki, M. Yokota, S. Yamawaki, Effect of Periodic Wake Passing on Film Effectiveness of Discrete Cooling Holes Around the Leading Edge of a Blunt Body, ASME. J. Turbomach. 119 (2) (1997) 292–301, doi:10.1115/1.2841112.
[18] M. Ochs, A. Schulz, H.-.J. Bauer, Investigation of the Influence of Trailing Edge Shock Waves on Film Cooling Performance of Gas Turbine Airfoils, ASME Turbo Expo (2007) Paper No. GT2007-27482, doi:10.1115/GT2007-27482
[19] H.J. Rehder, Investigation of Trailing Edge Cooling Concepts in a High Pressure Turbine Cascade – Aerodynamic Experiments and Loss Analysis, ASME J. Turbo mach. 134 (2012) 051029(1-11)
[20] de la Loma, G. Paniagua, D. Verrastro, P. Adami, Transonic Turbine Stage Heat Transfer Investigation in Presence of Strong Shocks, ASME. J. Turbomach. 130 (3) (2008) 031019, doi:10.1115/1.2777193.
[21] R.S. Abhari, G.R. Guenette, A.H. Epstein, M.B. Giles, Comparison of Time Resolved Turbine Rotor Blade Heat Transfer Measurements and Numerical Calculations, ASME, J. Turbomach. 114 (4) (1992) 818–827, doi:10.1115/1.2928035.
[22] R.S. Abhari, Impact of Rotor–Stator Interaction on Turbine Blade Film Cooling, ASME. J. Turbomach. 118 (1) (1996) 123–133, doi:10.1115/1.2836593.
[23] J. Schlienger, A.I. Kalfas, R.S. Abhari, Vortex-Wake-Blade Interaction in a Shrouded Axial Turbine, ASME. J. Turbomach. 127 (4) (2005) 699–707, doi:10. 1115/1.1934263.
[24] K.E. Ragab, L. El-Gabry, Heat Transfer Analysis of the Surface of Nonfilm-Cooled and Film-Cooled Nozzle Guide Vanes in Transonic Annular Cascade, ASME Turbo Expo (2017) Paper No. GT2017-64982, doi:10.1115/GT2017-64982.
[25] H. Xu, J. Wang, T. Wang, Numerical Investigations of Wake and Shock Wave Effects on Film Cooling Performance in a Transonic Turbine Stage: part 1 — Methodology Development and Qualification Over Stationery Stators and Rotors, ASME Turbo Expo (2013) Paper No. GT2013-94544, doi:10.1115/ GT2013-94544.
[26] H. Xu, J. Wang, T. Wang, Numerical Investigations of Wake and Shock Wave Effects on Film Cooling Performance in a Transonic Turbine Stage: part 2 — Unsteadiness Effect in a 2D Rotating Passage, ASME Turbo Expo (2013) Paper No. GT2013-94545, doi:10.1115/GT2013-94545.
[27] F.C. Kopper, R. Milano, R.D. Davis, R.P. Dririg, R.C. Stoeffler, Energy Efficient Engine High Pressure Turbine Component and Integration Program: High Pressure Turbine Supersonic Cascade Technology Report, NASA CR-165567 (1981).
[28] C.A. Hunter, Experimental, Theoretical and Computational Investigation of Separated Nozzle Flows, AIAA, 1998 Paper No. AIAA 98-3107, doi:10.2514/6. 1998-3107.
[29] Aalrebei, Odi Fawwaz, Anwar Hamdan Al Assaf, Abdulkarim Amhamed, Nedunchezhian Swaminathan, and Sally Hewlett. "Ammonia-hydrogen-air gas turbine cycle and control analyses." International Journal of Hydrogen Energy (2022).
[30] Okafor, Ekenechukwu Chijioke, Yuji Naito, Sophie Colson, Akinori Ichikawa, Taku Kudo, Akihiro Hayakawa, and Hideaki Kobayashi. "Measurement and modelling of the laminar burning velocity of methane-ammonia-air flames at high pressures using a reduced reaction mechanism." Combustion and Flame 204 (2019): 162-175.
[31] https://www.ansys.com/
[32] Borello, Domenico, DavideAnielli, Franco Rispoli, Alessandro Salvagni, and Paolo Venturini. "Unsteady CFD analysis of erosion mechanism in the coolant channels of a rotating gas turbine blade." In ASME Turbo Expo, pp. 15-19. 2015.
[33] Singh, Priyanka, and O. P. Shukla. "Heat transfer analysis of gas turbine rotor blade through staggered holes using CFD." International Journal of Engineering Research and General Science 4, no. 2 (2016).
[34] Brahmaiah, K. Hari, and M. Lava Kumar. "Heat transfer analysis of gas turbine blade through cooling holes." International Journal of Computational Engineering Research, ISSN (2014): 2250-3005.
[35] Butler, Robert J., Aaron R. Byerley, Kenneth VanTreuren, and James W. Baughn. "The effect of turbulence intensity and length scale on low-pressure turbine blade aerodynamics." International journal of heat and fluid flow 22, no. 2 (2001): 123-133
[36] Ansys. Ansys Cfx - Solver Theory Guide. Canonsburg: Ansys, Inc., 2013.
[37] Chen, Zhiqiang, and Yong Jiang. "Numerical investigation of the effects of H2/CO/syngas additions on laminar premixed combustion characteristics of NH3/air flame." International Journal of Hydrogen Energy 46, no. 21 (2021): 12016-12030.
[38] Bernardini, Matteo, I. Asproulias, J. Larsson, S. Pirozzoli, and F. Grasso. "Heat transfer and wall temperature effects in shock wave turbulent boundary layer interactions." Physical Review Fluids 1, no. 8 (2016): 084403.
[39] Zel'Dovich, Ya B., and Yu P. Raizer. Physics of shock waves and high-temperature hydrodynamic phenomena. Courier Corporation, 2002.
[40] Reising, Steffen, and Heinz-Peter Schiffer. "Non-axisymmetric end wall profiling in transonic compressors—Part I: Improving the static pressure recovery at off-design conditions by sequential hub and shroud end wall profiling." In Turbo Expo: Power for Land, Sea, and Air, vol. 48883, pp. 11-24. 2009.

[41] Mallick, Monalisa, Awadhesh Kumar, N. Tamboli, A. Kulkarni, P. Sati, V. Devi, and S. S. Chandra. "Study on drag coefficient for the flow past a cylinder." International Journal of Civil Engineering Research 5, no. 4 (2014): 301-306.
[42] Anderson, John David, and Mary L. Bowden. "Introduction to flight." (2005).
[43] Pope, Stephen B., and Stephen B. Pope. *Turbulent flows*. Cambridge university press, 2000.
[44] Iwata, Kotomi, TetsuroSekine, Izumi Tanaka, Takahiro Ando, and Erika Orita. "Turbulent Kinetic Energy Is Different from Viscous Energy Loss." RadioGraphics 40, no. 7 (2020): 2142-2144.